# Synthesis and Biological Studies on ‘Smart’ Iron Chelator Molecules

Young, Benjamin

*Award date:*
2013

*Awarding institution:*
University of Bath

# CHAPTER 2: RESULTS AND DISCUSSION (PART I)

## NPE, NV and DEACM-caged iron chelators.

2.1. NPE-caged iron chelators

By far the most extensively used group of PRPGs are those belonging to the 2-nitrobenzyl family, which have been the focus of extensive photochemical characterisation and research since they were first reported in the 1960s.[103] The simplest *ortho*-alkylated nitrophenyl PRPG is the *ortho*-nitrobenzyl moiety itself (see Figure 1.18, **I**) the photocleavage of which was first reported in 1966 by Schofield *et al*.[114] The 2-nitrobenzyl entity and its derivatives were first intended for use as protecting groups within organic synthesis by virtue of their facile and selective photolytic removal. Additionally, the stability of nitrobenzyl ethers makes them chemically unreactive to a wide range of conditions, which has made them especially useful for the synthesis of peptides as exemplified by Scheme 2.1.[115] Light-induced cleavage of the ONB group on tyrosine derivative **39** to liberate **40** and nitroso compound **26** offers a degree of orthogonality in that selective deprotection of the phenol can be achieved in the presence of the BOC protecting group and ethyl ester.

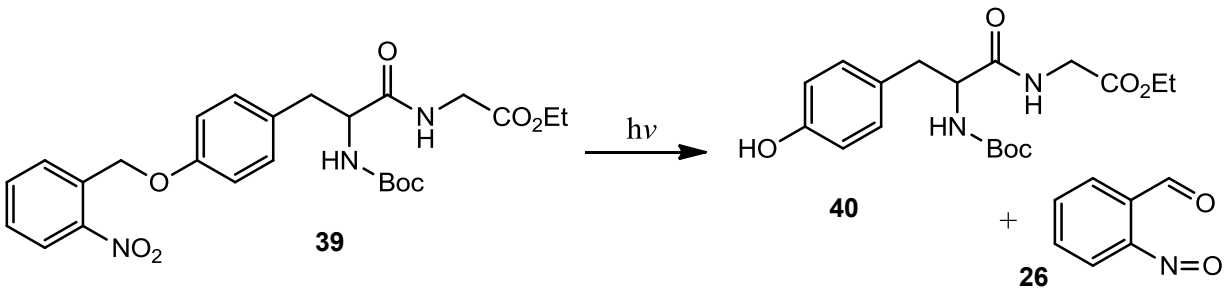


**Scheme 2.1.** Example of the ONB moiety as a protecting group and its orthogonal photoremoval.[115]

More significantly the benzyl-aryl ether bond is stable under physiological conditions; however the nitrosobenzaldehyde photoproduct **26** may be potentially harmful to biological systems,[100] which makes the 2-nitrobenzyl group unsuitable for use in a caged compound where the objective is to study its effect within a biological system.

A variation of this caging group is the 2-nitrophenylethyl (2-NPE) moiety (see Figure 1.18, **II**) which has a methyl group on the $\alpha$-carbon atom and has been shown to undergo significantly faster photolysis when irradiated at 365 nm.[116] Such rapid photolysis is valuable where caged molecules are designed for a biomedical

application, and the exposure time of tissue to potentially harmful activating light is therefore minimised. NPE photocleavage results in the generation of a nitrosophenylketone (NPK, **35**) as shown in Scheme 2.2. Although it has been reported that NPK undergoes reactions with thiol compounds,[117] to date there are no published *in vitro* studies which explicitly describe its toxicity in a particular cell line. The NPE moiety has been used as a PRPG in a variety of compounds, although one of the earliest examples is the carbamoylcholine derivative **41**, in which more unusually, the amide function is caged.[118]

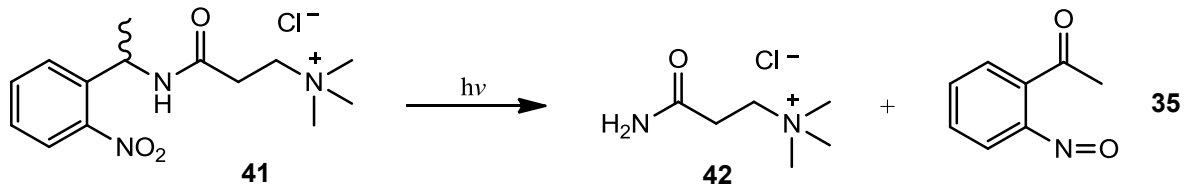


**Scheme 2.2.** One of the first reported NPE-caged compounds and its photolysis to yield NPK **35**.

The photochemical mechanism which describes *ortho*-nitrobenzyl caging group cleavage has been subject to extensive investigation, but is now generally accepted to proceed as shown with 2-NPE in Scheme 2.3.[101]

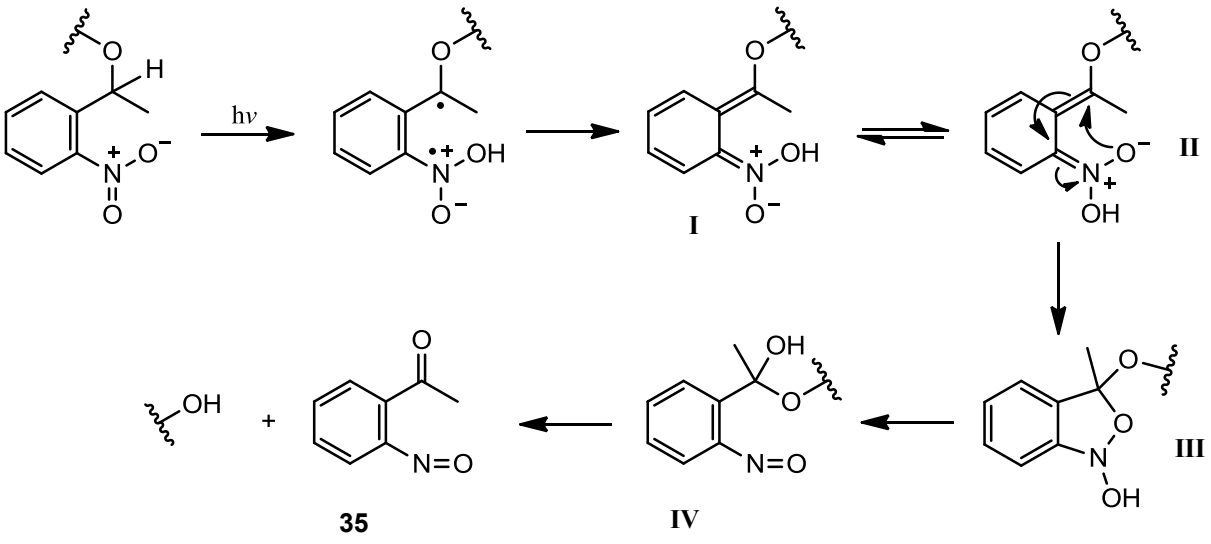


**Scheme 2.3.** Mechanism of NPE group photocleavage to produce NPK **35**.

It is established that photon capture leads to nitro group excitation, which subsequently removes a proton from the $\alpha$-carbon leading to intramolecular electron redistribution and formation of the *aci*-nitro tautomer **I**.[119] This nitronic acid species

exists in equilibrium between its two isomeric forms (**I** and **II**) through proton transfer; however the (*E*)-isomer **II** undergoes cyclisation to the benzisoxazoline intermediate **III** which subsequently collapses to the hemiacetal **IV**. Decomposition of **IV** to release the free alcohol along with NPK appears to be the rate limiting step to complete decaging, and also appears to be pH dependent, occurring much quicker under basic conditions.

Although generation of the *aci*-nitro tautomer is the only step which requires the input of light energy, caging groups with high quantum yields are more attractive for use in biomedical applications. The relatively fast photolysis of NPE has already been mentioned; however there is also scope for the design of caging groups which undergo photocleavage at longer wavelengths. It has been demonstrated that simple 2-nitrobenzyl caged compounds undergo faster release at shorter wavelengths within the UV region as one might expect based on their absorption spectra, which is demonstrated by tosylate derivative **43** (Scheme 2.4).[119]

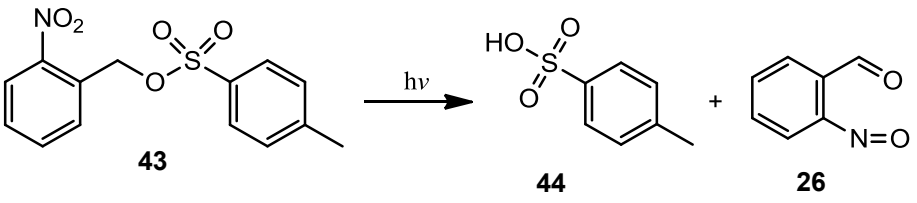


| λ (nm) | Release |
|---|---|
| 400 | 6% |
| 365 | 27% |
| 300 | 43% |

**Scheme 2.4.** Photorelease of TsOH **44** after irradiation of **43** at various wavelengths of light for 60 min.

Caging of the aroylhydrazones with the NPE group was achieved by chemical blockade of the phenolic oxygen (Scheme 2.5) as exemplified by NPE-PIH **34** below, which should undergo photolysis as shown. The phenol was chosen as the site of PRPG attachment because of the relative synthetic ease associated with phenol alkylation, and of course the critical iron-binding function of the phenolic oxygen.

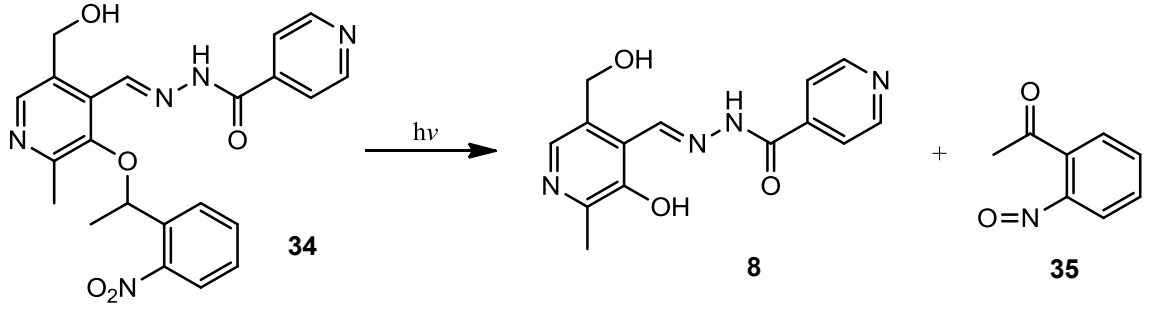


**Scheme 2.5.** Photolysis of the CIC **34** (NPE-PIH) to give 'naked' PIH, **8** and the NPK photofragment **35**.

Synthesis of the parent aroylhydrazone chelators, NIH (**11**) SIH (**10**) and PIH (**8**) was achieved by condensation of isonicotinic acid hydrazide (INH) with the corresponding aldehydes to form the hydrazone as described by Ponka *et al*. (Scheme 2.6).[72] The aldehyde precursors were 2-hydroxy-1-napthaldehyde, salicylaldehyde and pyridoxal hydrochloride (**45**-**47**) for NIH, SIH and PIH respectively.

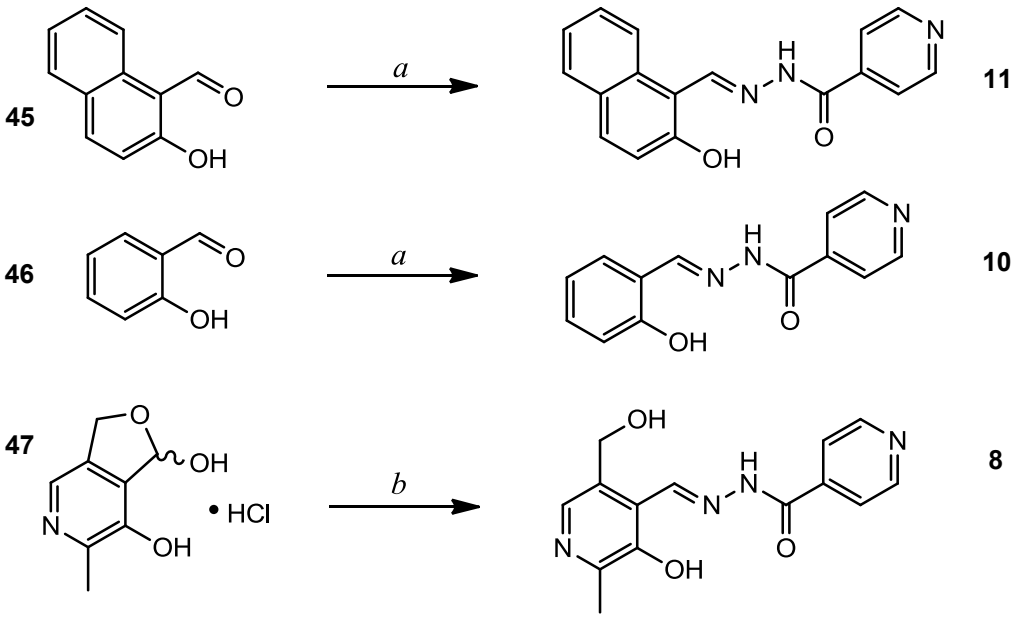


**Scheme 2.6.** Preparation of parent aroylhydrazone ICs **8**, **10** and **11**. *Reagents and conditions*: *a*. INH, EtOH, 85 °C, 3 h, **85-90%**; *b*. INH, NaOAc, 50% aq. EtOH reflux, 1 h, **77%**.

For the preparation of NPE-caged aroylhydrazones, O-alkylation of the phenolic oxygen was undertaken on the aromatic aldehyde prior to Schiff base formation. This strategy was adopted because of the relative structural simplicity of the aldehydes compared to their condensed hydrazone counterparts, the latter of which contain potentially nucleophilic nitrogen centres that have the potential to undergo additional transformations. NPE-attachment to aromatic aldehydes was achieved firstly by creation of a bromine handle on 1-ethyl-2-nitrobenzene **48** under Wöhl-Ziegler conditions to give the monobrominated benzyl product **49** in 57% yield (Scheme 2.7).[120] ABCN was employed as the radical initiator instead of AIBN, which was the agent of choice reported by Johnsson and colleagues. It was found as a consequence that the yield of **49** obtained was considerably lower than that reported in the literature (90%). O-alkylation of the 2-hydroxy aryl aldehyde with NPE was then achieved under basic conditions with caesium carbonate to give the 'caged' aldehyde derivatives **50**-**52** in 56-80% yield.

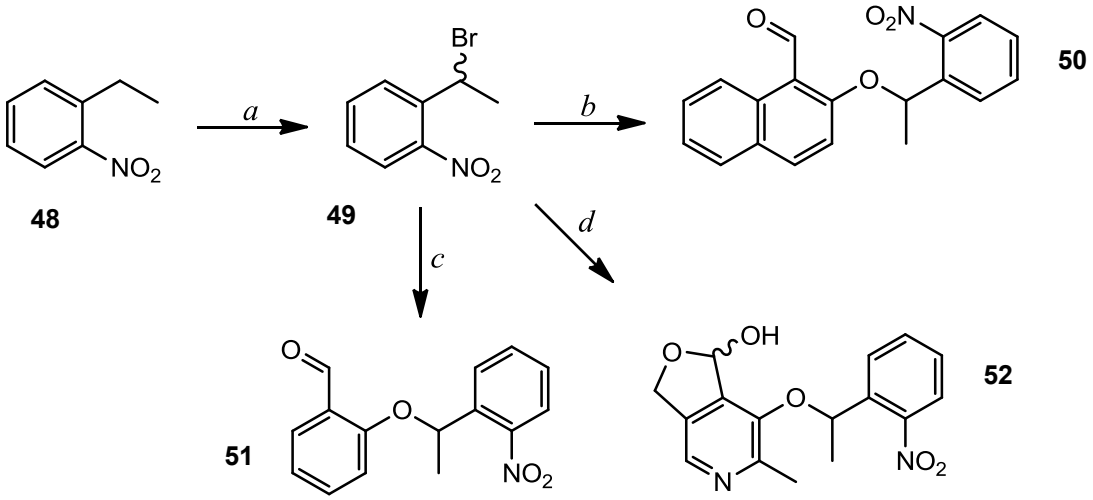


**Scheme 2.7.** Synthesis of O-NPE aldehydes **50-52**. *Reagents & conditions: a.* NBS, ABCN, $CCl_4$, reflux, 22 h, **57%**; *b*. 2-hydroxy-1-naphthaldehyde, $Cs_2CO_3$, 18-crown-6, DMF, RT, 24 h, **56%**; *c.* salicylaldehyde, conditions as with *b*, **80%**; *d*. pyridoxal HCl, conditions as with *b*, **68%**.

Subsequent condensation of the alkylated aldehydes with INH gave the corresponding NPE-caged aroylhydrazones in 32-66% yield (Scheme 2.8). Although these yields are somewhat modest, in all cases the compounds could be readily isolated in their pure form, free from unchanged aldehyde by either direct filtration from the reaction mixture, or by column chromatography. In the preparation of NPE-PIH **34**, this step was undertaken in the presence of DOWEX ion exchange resin to promote formation of the reactive 'open' aldehyde tautomeric form, thus allowing condensation to occur more efficiently (Scheme 2.9).

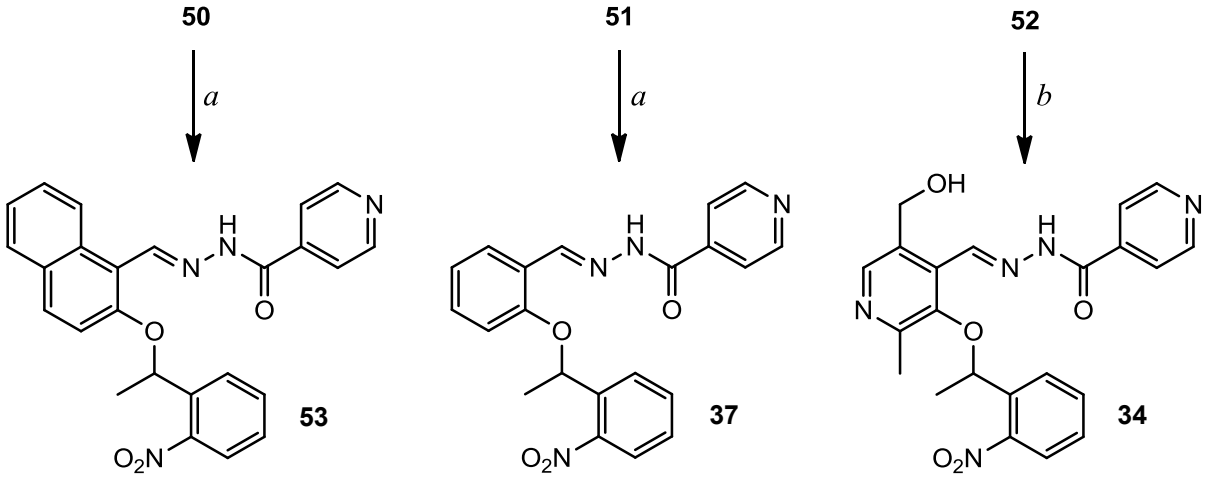


**Scheme 2.8.** Condensation reactions of INH and NPE-caged aldehydes. *Reagents and conditions: a.* INH, 90% aq. EtOH, reflux 22-24 h, **32%** (**53**) or **66%** (**37**); *b.* INH, DOWEX 50WX8-100, EtOH/$H_2O$ (9:1), reflux, 21 h, **38%**.

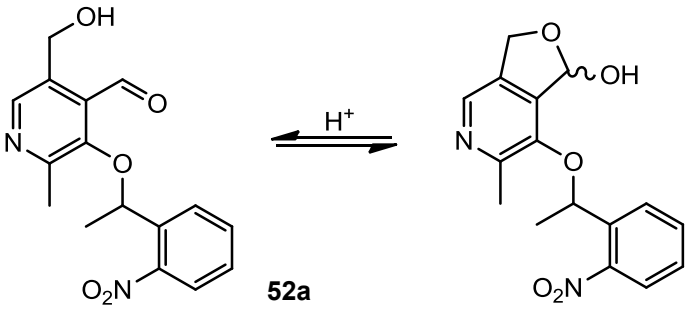


**52a** **52**

**Scheme 2.9.**

Tautomerism of pyridoxal, showing its 'open' aldehyde (**52a**) and cyclic furanol or hemiacetal form (**52**).

Synthesis of parent naphthylaldehyde thiosemicarbazone ICs **54a** and **54b** and their corresponding NPE-caged counterparts **55a** and **55b** was performed in a similar fashion to the aroylhydrazones by condensing 2-hydroxy-1-naphthaldehyde with the appropriate thiosemicarbazide (Table 2.2, Scheme 2.10, **A**). A thiohydrazone analogue of PIH, known as $H_2$PTBH (**56**), and its NPE-caged derivative **57** was also similarly prepared from pyridoxal (**47**) or the NPE-pyridoxal derivative **52** (**B**). The required precursor for this, thiobenzhydrazide **59**, was first prepared by hydrazinolysis of thioglycolic acid derivative **58** (**C**).[121]

**Table 2.2.**

| | R | X | Rx* | Yield |
|---|---|---|---|---|
| **54a** | $NMe_2$ | H | *a* | 75% |
| **55a** | $NMe_2$ | NPE | *a* | 65% |
| **54b** | $NH_2$ | H | *b* | 87% |
| **55b** | $NH_2$ | NPE | *b* | 39% |

| | X | Rx* | Yield |
|---|---|---|---|
| **56** | H | *d* | 87% |
| **57** | NPE | *d* | 37% |

∗ Rx = reaction conditions, see Scheme 2.10.

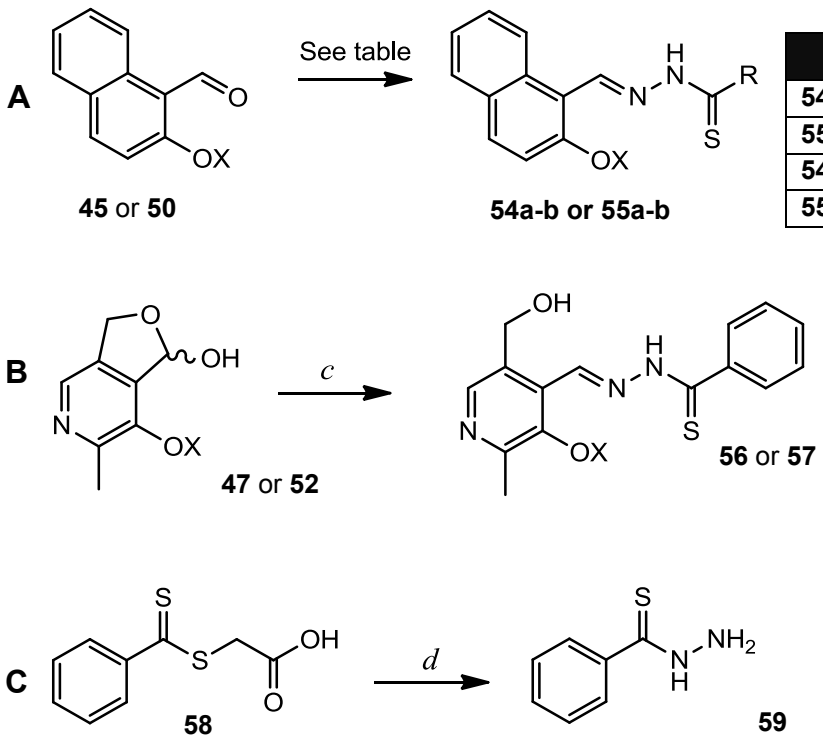


**45** or **50** **54a-b or 55a-b**

**47** or **52** **56** or **57**

**58** **59**

**Scheme 2.10.** Preparation of sulfur-containing ICs: NT44mT (**54a**), NT (**54b**) and $H_2$PTBH (**56**), along with their NPE-caged derivatives (**55a**, **55b** and **57** respectively). Also shown is the preparation of thiobenzhydrazide **59**. For yields, see Table. *Reagents and conditions:*

*a.* 4,4-dimethyl-3-thiosemicarbazide, EtOH, reflux, 3.5 h;

*b*. Thiosemicarbazide, EtOH, reflux, 5 h;

*c*. (i) Hydrazine monohydrate, 1 M NaOH, $H_2O$ (ii) 5 M HCl, 0 °C, 1 h, **98%**;

*d*. INH, DOWEX 50WX8-100, EtOH, reflux, 17 h.

The Schiff base CICs described above are sensitive to acid-catalysed hydrolysis when purified by column chromatography over silica gel; however it was found that this could be circumvented by adding to the eluent a small amount of pyridine (approx. 0.1%) which serves to neutralise the column, leading to improved product recoveries.

## 2.2. NV-caged iron chelators

It has been shown that substitution on the aryl ring of nitrobenzyl PRPGs can alter their absorption properties, which dictates the wavelength at which they undergo photoremoval with optimal efficiency.[122] The 3,4-dimethoxy-6-nitrobenzyl entity, also known as 6-nitroveratryl (NV, see Figure 1.18, **II**) was first introduced in 1970 by Woodward *et al*.,[123] and has been shown to absorb at longer wavelengths than other nitrobenzyl derivatives. In fact, the NV group is one of few PRPGs reported to work at low energy wavelengths as long as 420 nm.[113] Replacement of the position *para* to the nitro group on ring with an electron-withdrawing group however seems to have an opposing effect as shown in Figure 2.1).[124]

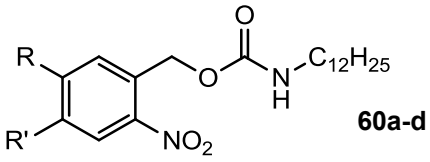


**60a-d**

**Figure 2.1.** Effects of aryl ring substitution on the photocleavage kinetics of a nitrobenzyl-caged compound.

| | R | R' | t ½ (254 nm) | t ½ (420 nm) |
|---|---|---|---|---|
| **60a** | OMe | OMe | 98 min | 330 min |
| **60b** | H | H | 47 min | 420min |
| **60c** | Cl | H | 27min | 481min |
| **60d** | Br | H | 29 min | 578 min |

The longer wavelength absorption profile of NV was originally designed for use with amino acids such as tryptophan and tyrosine, which are sensitive to shorter wavelengths within the UV spectrum.[113] These properties also make NV attractive for use in the preparation of CICs, as its absorption profile,[124] suggests that photocleavage should occur more efficiently following exposure to UVA light compared to NPE-caged compounds. It is also important as longer wavelengths of light, which are lower in energy are able to penetrate deeper into tissue. This may be particularly relevant for CICs which may have applications as photoprotective agents, although a possible problem is the liberation of potentially harmful nitrosobenzaldehyde photoproduct **61** (Scheme 2.11). Nevertheless, photochemical comparison of ICs which are caged with NPE and NV should provide some insight into how variation of the caging moiety can provide scope for “fine-tuning” their photorelease characteristics, and thus help in the rational design of CICs which are optimally active within the UVA range.

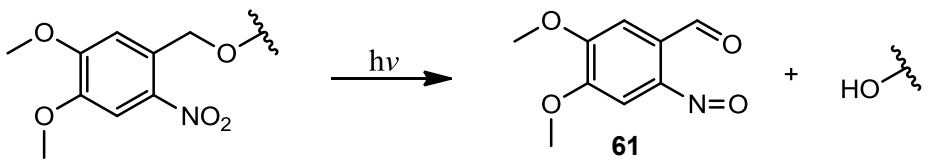


**Scheme 2.11.** Photocleavage of an NV-caged alcohol to release the free alcohol and the accompanying nitrosobenzaldehyde photoproduct **61**.

In similar fashion to the NPE group, the preparation of NV-caged aroylhydrazones SIH and PIH was achieved through attach ment of the PRPG to the phenolic oxygen. This began with synthesis of 6-nitroveratryl bromide **63** from nitroveratryl alcohol **62** using $PBr_3$ in anhydrous DCM (Scheme 2.12). It was anticipated that O-alkylation could be accomplished with the conditions used previously with the NPE group; however the expected product **64** was not observed when this reaction was attempted with salicylaldehyde. Although TLC showed complete consumption of starting material to a single new product, $^1$H NMR was not consistent with that expected for **53**, and lacked the characteristic resonance of the aldehyde proton.

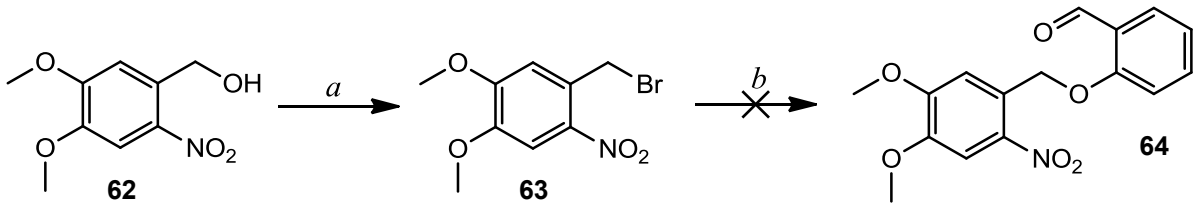


**Scheme 2.12.** Preparation of nitroveratryl bromide **63** and initial O-alkylation attempts. *Reagents and conditions: a.* $PBr_3$, anhydrous DCM, RT → reflux, 3 h, **77%**; *b*. salicylaldehyde, $Cs_2CO_3$, 18-crown-6, DMF, overnight, RT.

A possible explanation is that the alkylated product, once formed, undergoes a subsequent base-induced intramolecular aldol reaction to give a benzofuranyl derivative. This is discussed in more detail in section 2.3 (see Figure 2.16). Indeed, deprotonation of the benzylic protons in nitrobenzyl groups is not without precedent, as Poggi and coworkers have described the enhanced acidity of the nitrobenzyl methylene group within a nickel-complexed scorpionate system.[125] It is therefore feasible that such an active methylene group could then attack the nearby aldehydic carbon.[126]

In view of this result, an alternative alkylation procedure according to Miranda *et al.*[127] was therefore employed with the milder base, $K_2CO_3$,[128] and an increased

stoichiometric ratio of bromide **63** relative to the aldehyde (Scheme 2.13). The results of this methodology change were drastic, and the expected benzyl-aryl ethers were furnished in 99% (**64**) or 37% (**65**) yield. Subsequent condensation with INH as described previously gave the corresponding Schiff base aroylhydrazones in 68% or 26% yield for the SIH (**66**) and PIH (**67**) derivatives respectively. The low yield obtained for the NV-caged PIH was again a consequence of incomplete reaction progression, with 42% unchanged aldehyde also recovered following column chromatography. This was the same reason for the low yield of **65**.

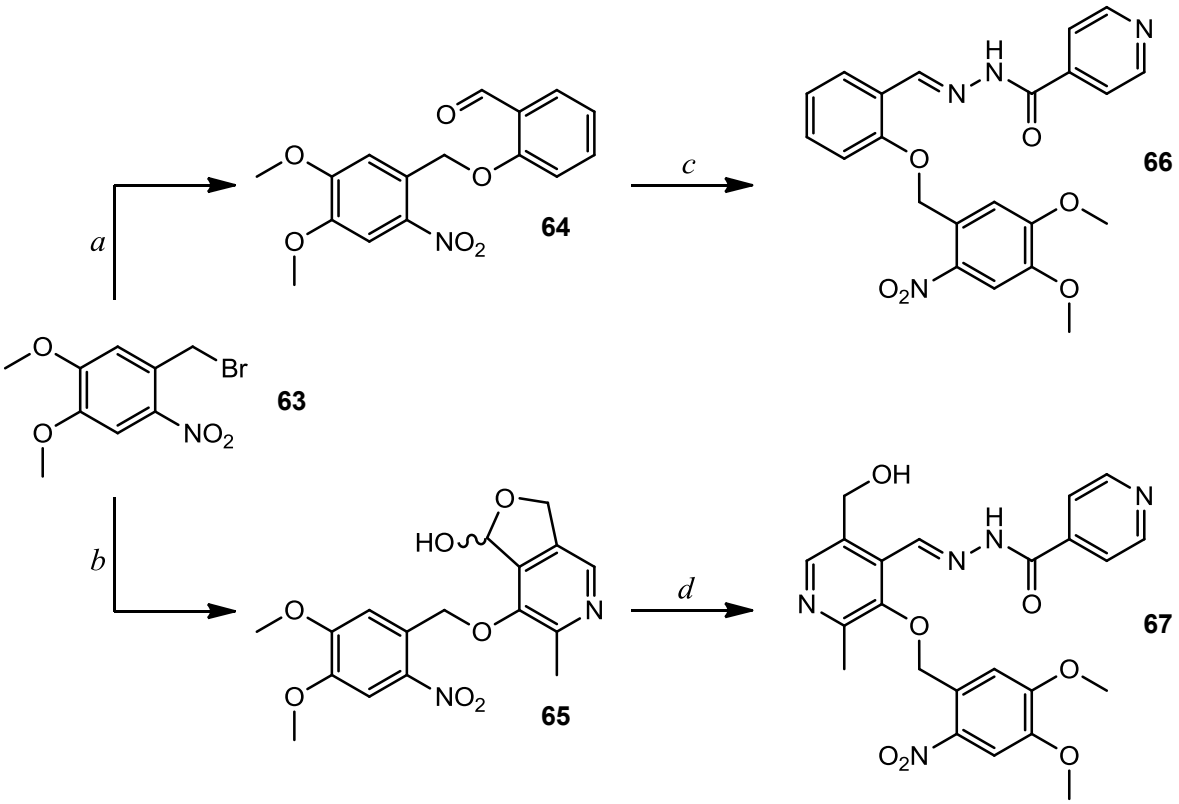


**Scheme 2.13.** Synthesis of NV-caged aroylhydrazone ICs **66** and **67**.
*Reagents and conditions:*
*a*. salicylaldehyde, $K_2CO_3$, $Me_2CO$, reflux, 5 h, **99%**;
*b*. pyridoxal hydrochloride, $K_2CO_3$, $Me_2CO$, reflux, 5 h, **37%**;
*c*. INH, 90% aq. EtOH, reflux, 1 h, **68%**;
*d*. INH, DOWEX 50WX8-100, 90% aq. EtOH, reflux, overnight, **26%**

## 2.3. Coumarin-4-yl-caged iron chelators

A third group of PRPGs, structurally unrelated to the *ortho*-nitrobenzyl caging groups which have been the subject of extensive investigation, are the coumarin-4-yl moieties. A considerable number of caged compounds, many of them phosphate-caged nucleotides[129] have been reported, as well as thiols[130] and alcohols.[131] Chemical attachment of coumarinyl PRPGs to molecules is commonly achieved by way of an ester or phosphate ester linkage (Figure 2.2), but has also been achieved through a carbonate or carbamate spacer depending on the type of functional groups involved.[100]

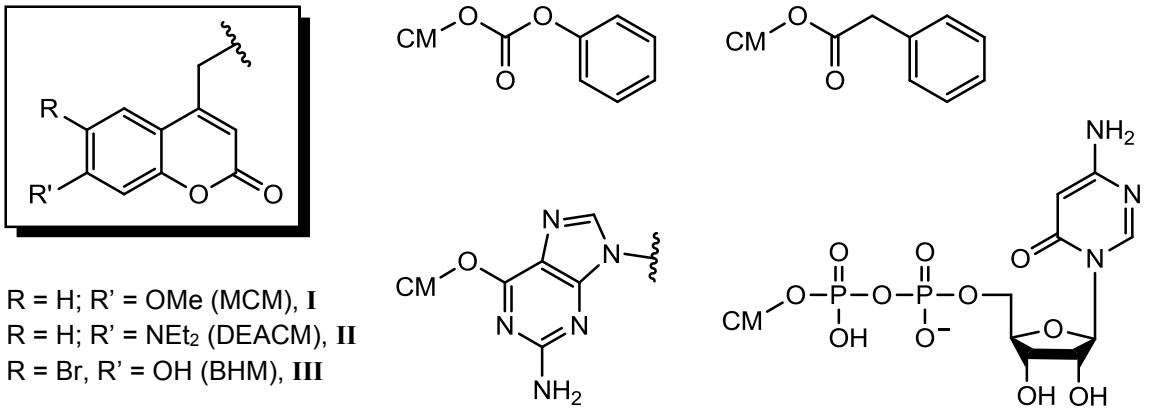


R = H; R' = OMe (MCM), **I**
R = H; R' = $NEt_2$ (DEACM), **II**
R = Br, R' = OH (BHM), **III**

**Figure 2.2.** Examples of coumarinyl caged compounds, depicting various functional groups through which attachment of the coumarin moiety can occur.

The appeal of the coumarinyl system as PRPGs stems from the high absorption coefficients and rapid photorelease that is often observed upon irradiation. Substituents on the C6 and C7 positions of the ring are established to have a significant impact on the photochemical properties of the coumarin chromophores and their caged counterparts. The three most commonly encountered coumarinyl PRPGs (see Figure 2.2) are the (7-methoxycoumarin-4-yl)methyl (MCM, **I**), (7-diethylaminocoumarin-4-yl)methyl (DEACM, **II**), and (6-bromo-7-hydroxycoumarin-4-yl)methyl (BHC, **III**), and the latter two exhibit especially interesting photochemical behaviour.[132] For instance BHC shows the highest photolytic quantum yields known for the coumarin-type groups,[131] while 7-DEACM absorbs at the most red-shifted wavelengths, with a $\lambda_{max}$ of some DEACM-caged compounds as high as 450 nm.[133] This makes DEACM especially appealing for use within CIC preparation, as uncaging

should occur efficiently upon exposure to light within the relatively low-energy UVA and visible light region. It also attractive from a synthetic perspective as unlike BHC which contains a phenolic hydroxyl function, there is no need to employ additional protecting group measures.

The range of caging groups which are compatible with the coumarin-4-yl PRPG however are limited, for instance aliphatic ethers which result from the caging of non-phenolic alcohols do not undergo photolysis. However, light-induced cleavage has been accomplished with more electron-rich ether systems such as caged diols[134] and with aryl ethers such as those seen with caged purines[132] (see Figure 2.2.) This is because photocleavage occurs through solvent-assisted photoheterolysis (Scheme 2.14) which can only take place when acidic functional groups are caged.[135] It was therefore expected that DEACM should be a promising caging group for CICs belonging to the aroylhydrazone family of iron chelators.

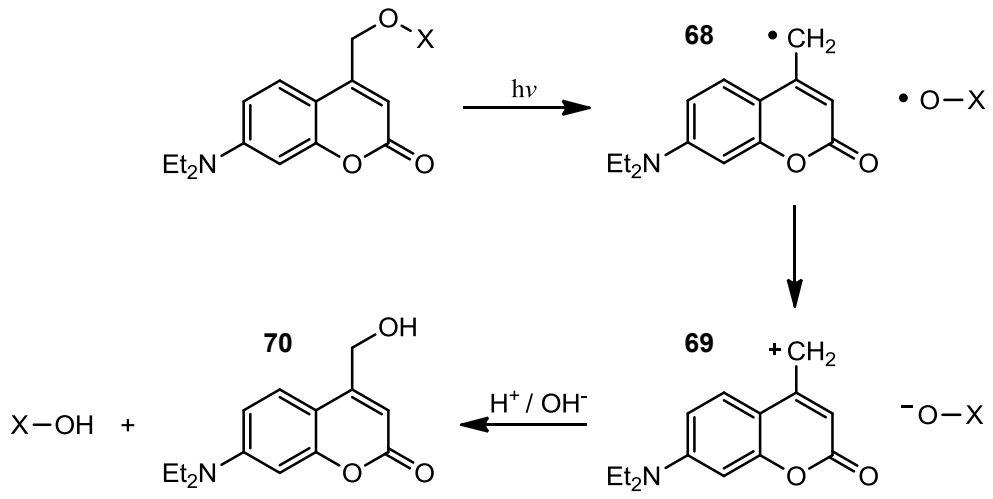


**Scheme 2.14.** Mechanism of photocleavage of the coumarin-4-ylmethyl caging group, exemplified by DEACM to give the coumarin-4-ylmethyl alcohol **70**.[135]

The preparation of DEACM-caged aroylhydrazones started from 7-diethylamino-4-methylcoumarin **71**, which underwent oxidation at the allyl-activated methyl group with selenium dioxide to form the corresponding aldehyde **72** in 35% yield (Scheme 2.15). This was subsequently reduced to the hydroxymethyl alcohol **70** using sodium borohydride, followed by bromination via the mesylate intermediate which gave the coumarin-4-ylmethyl derivative **73** with a reactive bromine handle for subsequent O-

alkylation. Unfortunately, the conditions for O-alkylation that were adopted for the NV group failed when applied to bromocoumarin **73** and salicylaldehyde; however, alkylation of pyridoxal proceeded to give **74** in a satisfactory yield of 46% under these conditions, and subsequent condensation with INH as described previously furnished the DEACM-caged PIH derivative **75**. Changing the solvent to DMF or adjusting the stoichiometry ratios of the coumarinyl bromide and/or base gave no improvement with attempted salicylaldehyde alkylation and **76** was not observed.

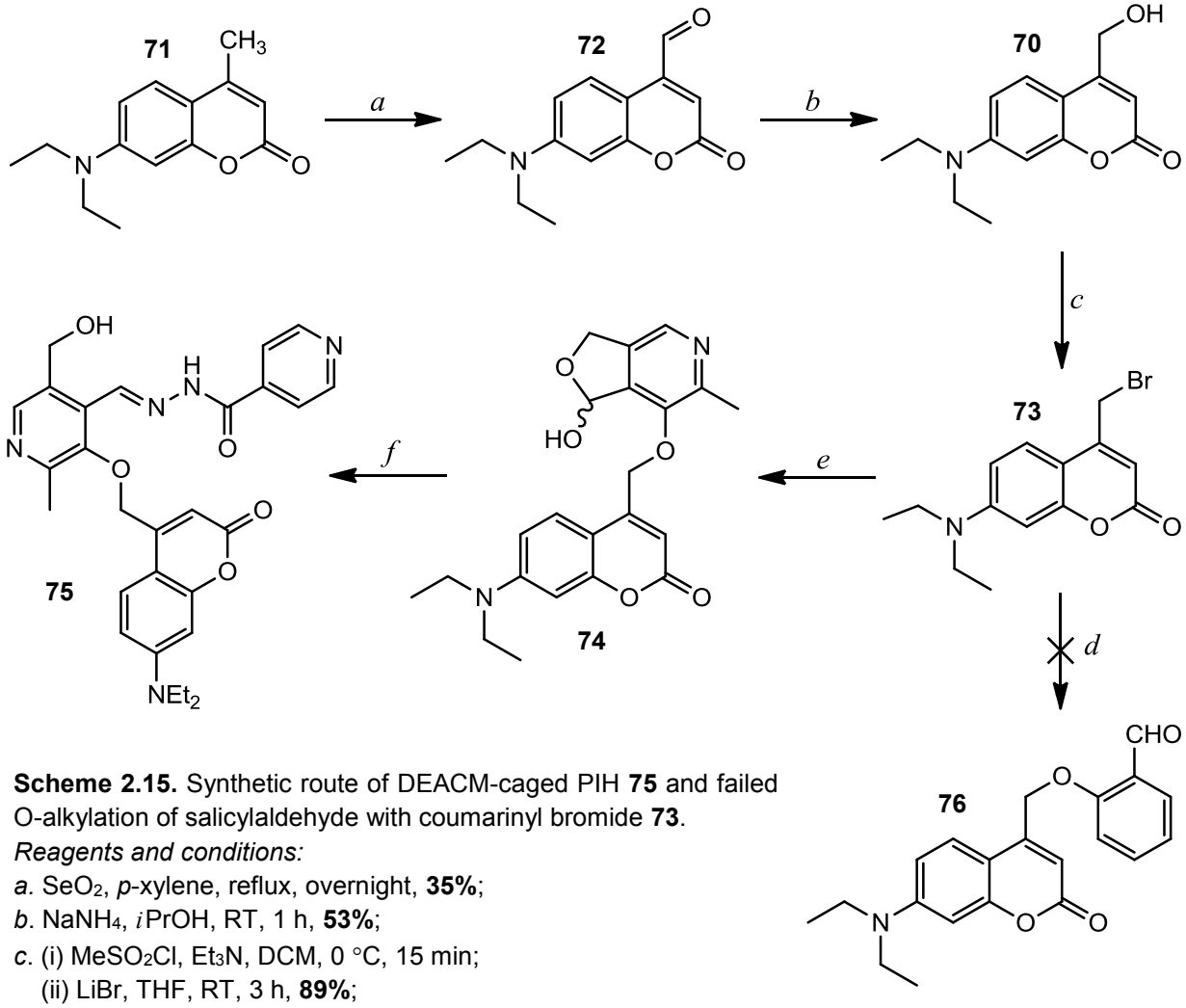


**Scheme 2.15.** Synthetic route of DEACM-caged PIH **75** and failed O-alkylation of salicylaldehyde with coumarinyl bromide **73**.
*Reagents and conditions:*
*a.* $SeO_2$, *p*-xylene, reflux, overnight, **35%**;
*b*. $NaNH_4$, *i*PrOH, RT, 1 h, **53%**;
*c*. (i) $MeSO_2Cl$, $Et_3N$, DCM, 0 °C, 15 min;
(ii) LiBr, THF, RT, 3 h, **89%**;
*d*. salicylaldehyde, $K_2CO_3$, $Me_2CO$ or DMF, reflux, 2-5 h;
*e*. pyridoxal HCl, $K_2CO_3$, $Me_2CO$, reflux, 5 h, **46%**.
*f*. INH, DOWEX 50WX8-100, 90% aq. EtOH, reflux, overnight, **16%**

One possible explanation for the difficulty in alkylating salicylaldehyde under these conditions is the occurrence of a base-catalysed intramolecular aldol reaction which results in the formation of a benzofuranyl product (Scheme 2.16), which has been reported by Ghate *et al*. who had employed similar conditions with both aldehyde and

coumarin substrates.[126] Indeed, this would explain why pyridoxal was able to undergo alkylation with **73** to give the expected ether product, as it exists entirely in its furanol form, thus meaning the aldehyde is "protected" from any attack by the activated methylene group.

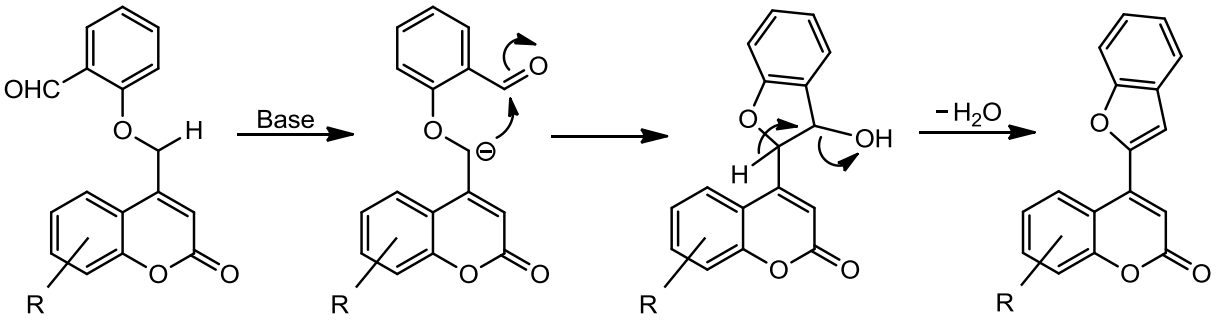


**Scheme 2.16.** Mechanism of the intramolecular aldol reaction and the resulting formation of a benzofuranyl derivative which may account for O-alkylation failure.[126]

As an alternative approach, we attempted to attach the DEACM group to the phenolic function of salicylaldehyde by activating the coumarinyl alcohol **70** under Mitsunobu conditions[132] (Scheme 2.17). However this proved unfruitful, and the expected aryl ether **76** was not isolated as no conversion was observed by TLC analysis.

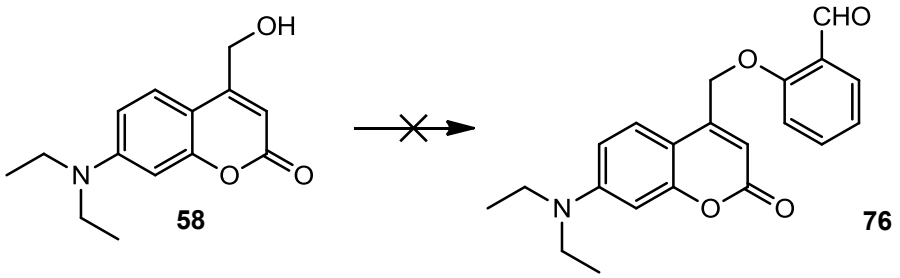


**Scheme 2.17.** Attempted attachment of the DEACM group to phenolic oxygen under Mitsunobu conditions. *Reagents and conditions:* salicylaldehyde, DEAD, $PPh_3$, THF, RT, overnight.

With the formation of a coumarin-4-ylmethyl-aryl ether proving difficult, we also considered the possibility of caging the phenolic aldehydes with the DEACM group through a carbonate ester, a route which is frequently employed in the synthesis of coumarinyl-caged compounds. This was attempted with salicylaldehyde and coumarinyl alcohol **70** as shown in Scheme 2.18, via formation of the *para*-nitrophenyl carbamate-ester intermediate as described by Hagen *et al*.[136] Although a new product was detected by TLC analysis, the expected product (**77**) was not isolated following column chromatography.

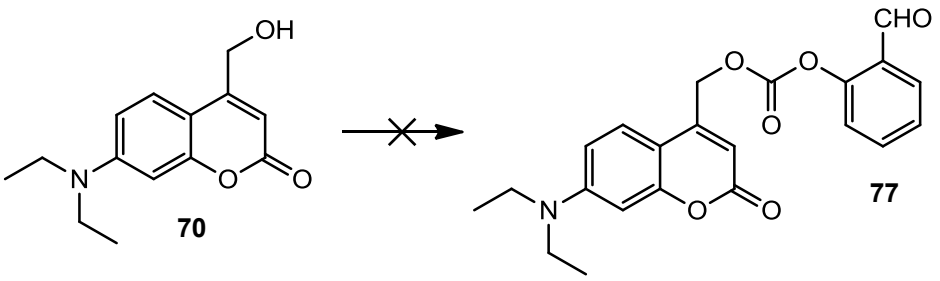


**Scheme 2.18.** Attempted O-alkylation of salicylaldehyde with DEACM by formation of a carbonate ester **77**. *Reagents and conditions*: (i) *para*-nitrophenyl chloroformate, DMAP, DMF, RT, overnight (ii) salicylaldehyde, DMAP, RT, overnight.

Based on the apparent base sensitivity of the coumarinyl derivative of salicylaldehyde (**76**), we finally attempted to design a set of alkylation conditions under which any excess of base could be avoided, thus minimising the risk of unwanted intramolecular aldol product formation. Ríos *et al*. have reported the alkylation of phenolic aldehydes with potassium *tert*-butoxide as a base, a method which was therefore implemented but with some slight modifications.[137] In particular, a sub-stoichiometric amount of base was used in this reaction (0.9 equiv.) relative to the phenolic substrate. A solution of potassium *tert*-butoxide in THF, obtained commercially, was employed which allowed for a much tighter level of control in the amount of base used. It was then anticipated that 'pre-formation' of the salicylaldehyde phenoxide anion, followed by subsequent slow addition of the deprotonated species to a solution of excess bromomethylcoumarin **73** should prevent any base-catalysed intramolecular-aldol products. This method proved successful, and the expected ether **76** was produced in 48% yield, which was subsequently condensed as described previously to give the complete DEACM-caged IC **78** in 54% yield (Scheme 2.19).

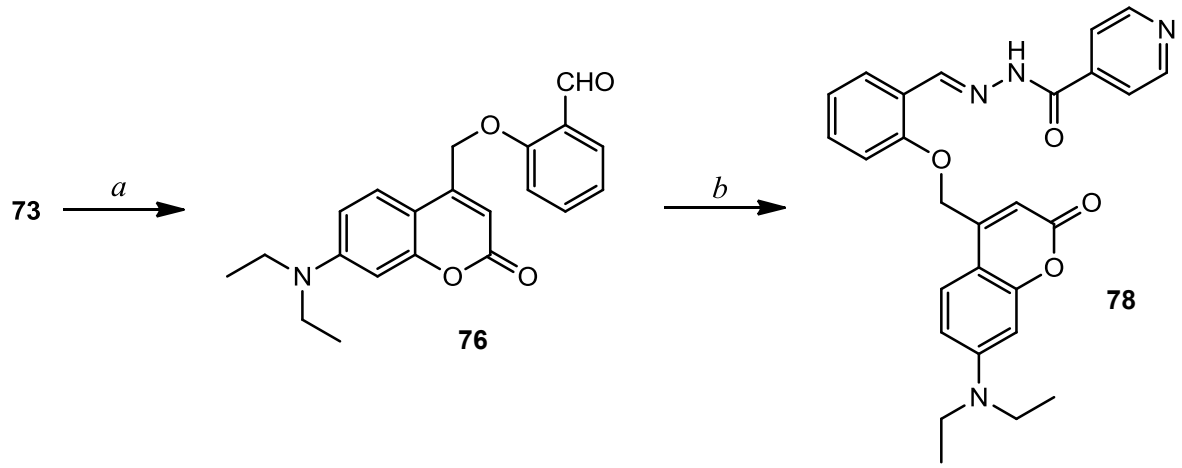


**Scheme 2.19.** Successful base-catalysed formation of benzyl-aryl ether **76** from bromomethyl coumarin **73** and subsequent aroylhydrazone **78** formation. *Reagents and conditions*: *a*. Salicylaldehyde, *t*BuOK, THF, RT, 2 min, then slow addition of mixture to **73** in THF, 50 °C, 3 h, **48%**; *b*. INH, 90% aq. EtOH, reflux, 2 h, **54%**.

## 2.4. Synthesis of NPK

In addition to the synthesis of NPE-CICs, it was decided that it would be useful to obtain NPK (**35**) which is produced from the photolysis of NPE-CICs. This is for two reasons: firstly, it would allow us to establish a retention time for this compound by HPLC analysis, thus establishing an invaluable reference marker for the analysis of NPE-CIC uncaging following irradiation. Secondly, it would allow us to directly evaluate its *in vitro* biological activity in a relevant biological system, such as keratinocyte skin cells, which to our knowledge has never been studied. The latter point is particularly important, as any cell killing observed upon decaging can then be reliably attributed to release of the active IC component.

To attain NPK, one possible strategy is to synthesise it photochemically; whereby an NPE-caged compound is irradiated and the nitrosoketone by-product is isolated by chromatography. A problem with this approach however is that a relatively large amount of caged compound would be required to obtain an adequate amount of nitrosoketone. Also if uncaging does not occur cleanly, then purification by column chromatography may prove difficult. We therefore decided to prepare NPK non-photochemically using the route depicted in Scheme 2.20. This was accomplished easily, from the commercially available nitrophenyl alcohol **79**, which when converted to the mesylate underwent subsequent base-catalysed elimination to nitrostyrene **80**.[138] Treatment with strong acid protonates the vinyl bond and results in formation of a carbocation formation which is subsequently attacked by the nitro oxygen.[139] The intramolecular rearrangement that follows affords nitroso ketone **35** in 61% yield.

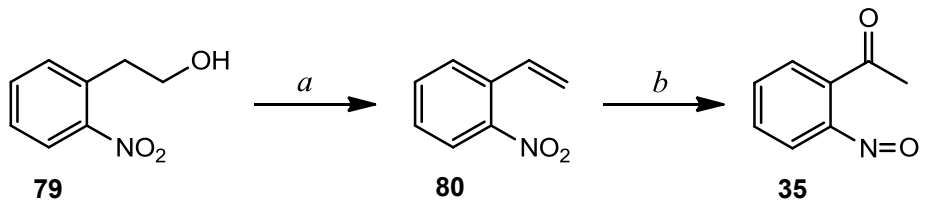


**79** **80** **35**

**Scheme 2.20.** Non-photochemical synthesis of NPK **35**. *Reagents and conditions*: *a.* $MeSO_2Cl$, DBU, THF, 0 °C → RT, 16 h, **96%**; *b*. $H_2SO_4$ (conc.), –10 °C, 50 min, **61%**.

## 2.5. Decaging experiments

### *2.5.1. General information*

Removal of the NPE, NV and DEACM caging groups from CICs by irradiation with UV light to release the active aroylhydrazone CIC and NPK fragment ("decaging") was performed on all CICs described.

Decaging experiments were originally performed with CIC solutions in MeCN; however with some compounds it was found that solubility of the CIC and/or the resulting photoproducts was too poor in this solvent. DMSO was therefore used as the solvent of choice, with CICs, reference ICs and all photoproducts possessing full solubility in this solvent at the concentrations used, namely 0.05% w/v.

Irradiation was conducted with a broad-spectrum Sellas 4kW UVA lamp which emits primarily within the UVA range (350-400 nm); however there is also low-level emission within the near-visible range above 400 nm. The emission spectrum of the lamp is shown in Figure 2.3.

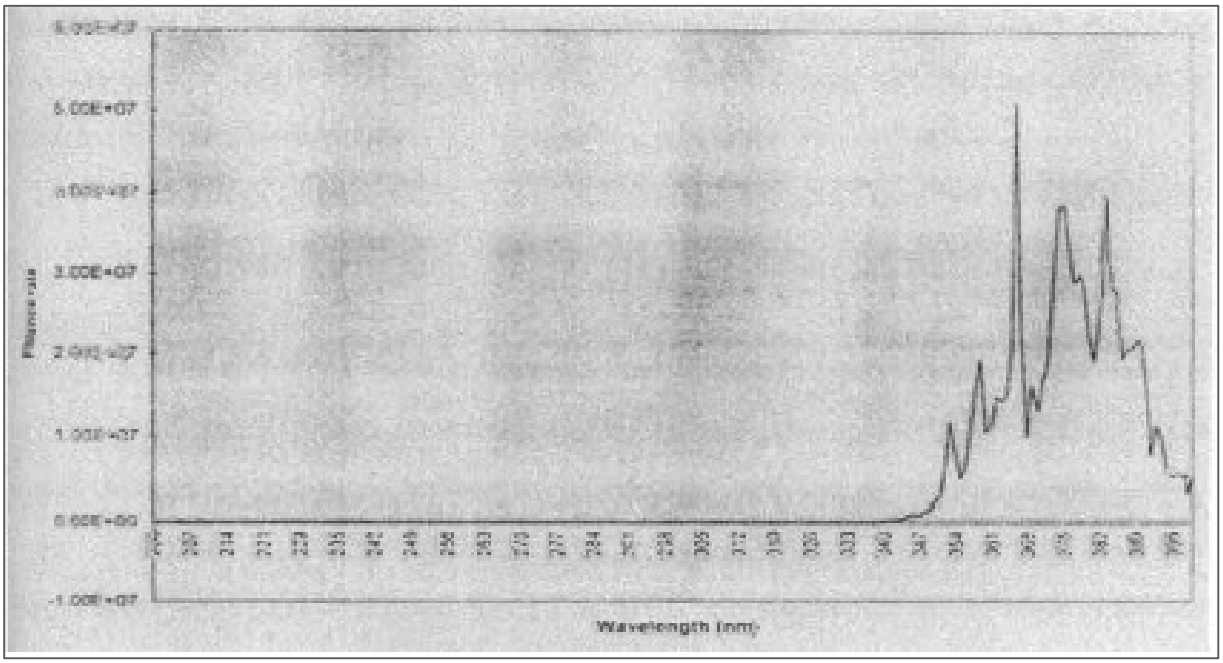


**Figure 2.3.** Emission spectrum of the Sellas UVA lamp used for decaging experiments.

CICs were exposed to a UV dose of 250 kJ/m$^2$. This is roughly equivalent to an exposure time of 70 minutes midday sunlight, during the summer at northern latitude

of 30-35 degrees.[140] This dose of UVA was selected as it is considered to be physiologically relevant, and therefore reflects a level of exposure which is likely to elicit damage to skin tissue without solar protection. It is also a level of exposure which people are likely to encounter throughout various parts of the world, and should provide an adequate level of energy for the photolysis of CICs to take place.

Approximately 1 hour post-irradiation, samples were characterised by HPLC analysis, detecting at a wavelength of 280 nm (unless otherwise stated) and compared to corresponding reference samples as appropriate.

*2.5.2. UV absorption spectra*

The UV absorbance profiles of all compounds described within this chapter were measured and recorded, including the $\lambda_{max}$ and molar absorption coefficient $\varepsilon$. For experimental details and methodology, see section 6.3. For UV absorbance data of individual compounds, see under the relevant compound in section 6.2.

Figure 2.4 shows the UV absorbance spectrum for three caged-PIH derivatives, namely the NPE, NV and DEACM-caged compounds **34**, **67** and **75** respectively. As expected, the DEACM-caged compound **75** shows considerably red-shifted absorption compared to its NPE and NV counterparts, with absorption maxima at 381 nm. In contrast, relative to the NPE-caged compound the NV-PIH derivative also shows a slight bathochromic shift (296 and 300 nm respectively). This pattern was also replicated in the corresponding SIH derivatives (data not shown).

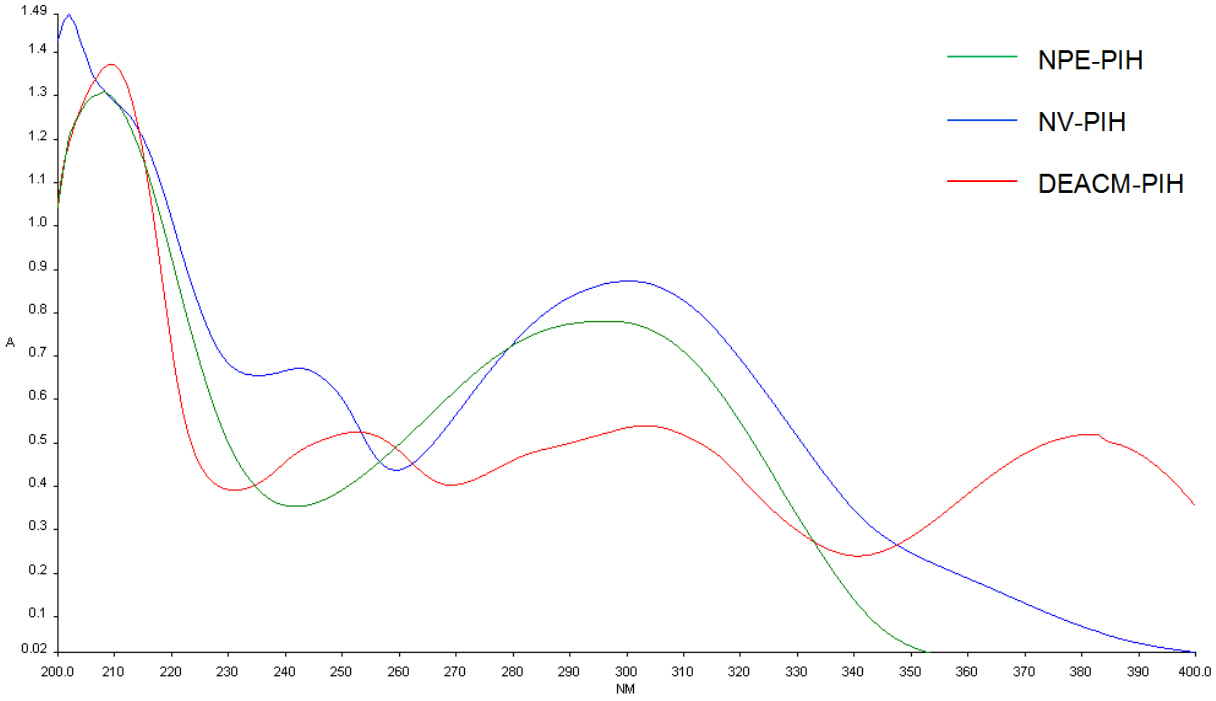


**Figure 2.4.** UV absorption profiles of the three caged PIH derivatives: NPE-PIH **34**, NV-PIH **67** and DEACM-PIH **75** at a concentration of 40 μM.

*2.5.3. Stability of parental ICs to UVA light*

The stability of the parental ("naked") ICs **8**, **10**-**11**, **54a-b** and **56** to UVA light were evaluated by dissolving in DMSO at a concentration of 0.05% w/v and irradiating at a dose of 250 kJ/m$^2$.

The ICs showed no evidence of UVA-induced degradation, except for the two thiosemicarbazone ICs **54a-b**, where the emergence of a weak signal suggested minor degradation (Figure 2.5).

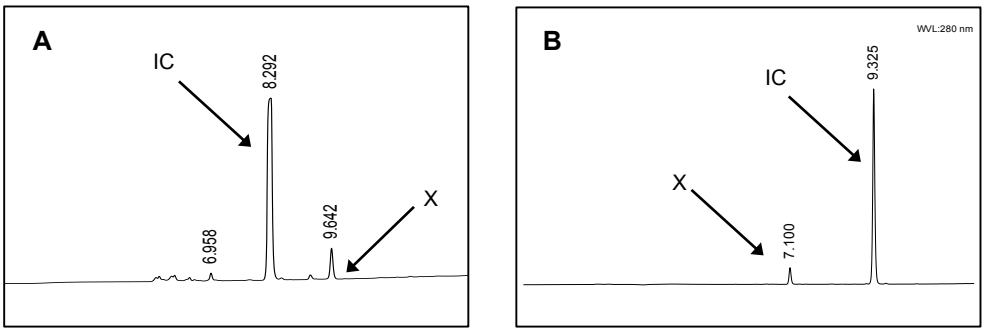


**Figure 2.5.** HPLC chromatograms of thiosemicarbazone ICs **54a** (**A**) and **54b** (**B**) following exposure to ambient light.. Possible degradation product signals are labelled 'X'.

*2.5.4. Stability of NPE-caged iron chelators to visible light*

Ideally, CICs should be resistant to photolysis by radiation within the visible light region of the electromagnetic spectrum (380-740 nm), as premature uncaging in ambient light would circumvent the current objective of producing context-specific iron chelation.

In order to evaluate their stability to ambient light, all NPE, NV and DEACM-caged ICs described in this chapter were dissolved in DMSO at a concentration of 0.05% w/v and allowed to stand overnight (15-16 h) in the fume hood under normal light emitted by a fluorescent lamp at RT. We anticipated that this should mimic a typical daily level of indoor, non-solar visible light that human skin is exposed to.

Analysis of the samples by HPLC showed no photolysis or uncaging under these conditions for any of the compounds, thus indicating the stability of the NPE, NV and DEACM group to ambient light.

*2.5.5. Uncaging of NPE-caged aroylhydrazones*

Figure 2.6 shows the uncaging profile for NPE-SIH, the HPLC chromatogram for which is shown under normal conditions (**A**) and 1 hour after irradiation with UVA (**B**). It can be seen that at this dose of UVA radiation, the caged compound appears to undergo complete photolysis, as the chromatogram signal for **37** is no longer observed in the irradiated sample. Furthermore, two new signals are generated which appear to correlate with the chromatogram profiles of SIH **10** (**C**) and NPK **35** (**D**), which is further confirmed by co-injection of the irradiated sample with either SIH (**E**) or NPK (**F**).

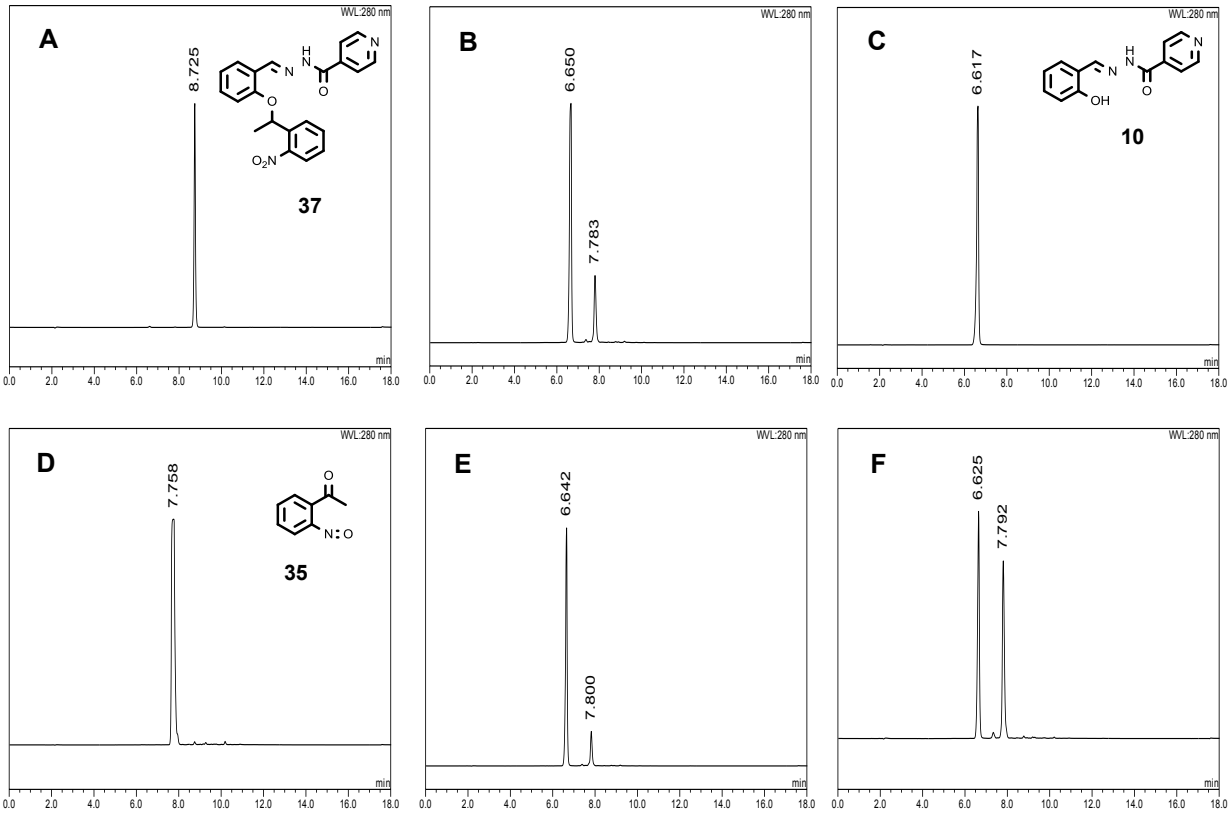


**Figure 2.6.** HPLC chromatograms of NPE-SIH **37** and its photoproducts, depicting the caged compound (**A**) and the UVA irradiated (250 kJ/m$^2$) compound (**B**). Also shown for reference is the 'naked' IC molecule SIH (**C**) and NPK (**D**) as well as co-injection of the irradiated sample with either SIH (**E**) or NPK (**F**).

NPE-PIH **34** exhibits the same decaging behaviour as SIH, with full release of the iron chelator and the NPK fragment (Figure 2.7), although some very minor side photoproducts appear to also be present.

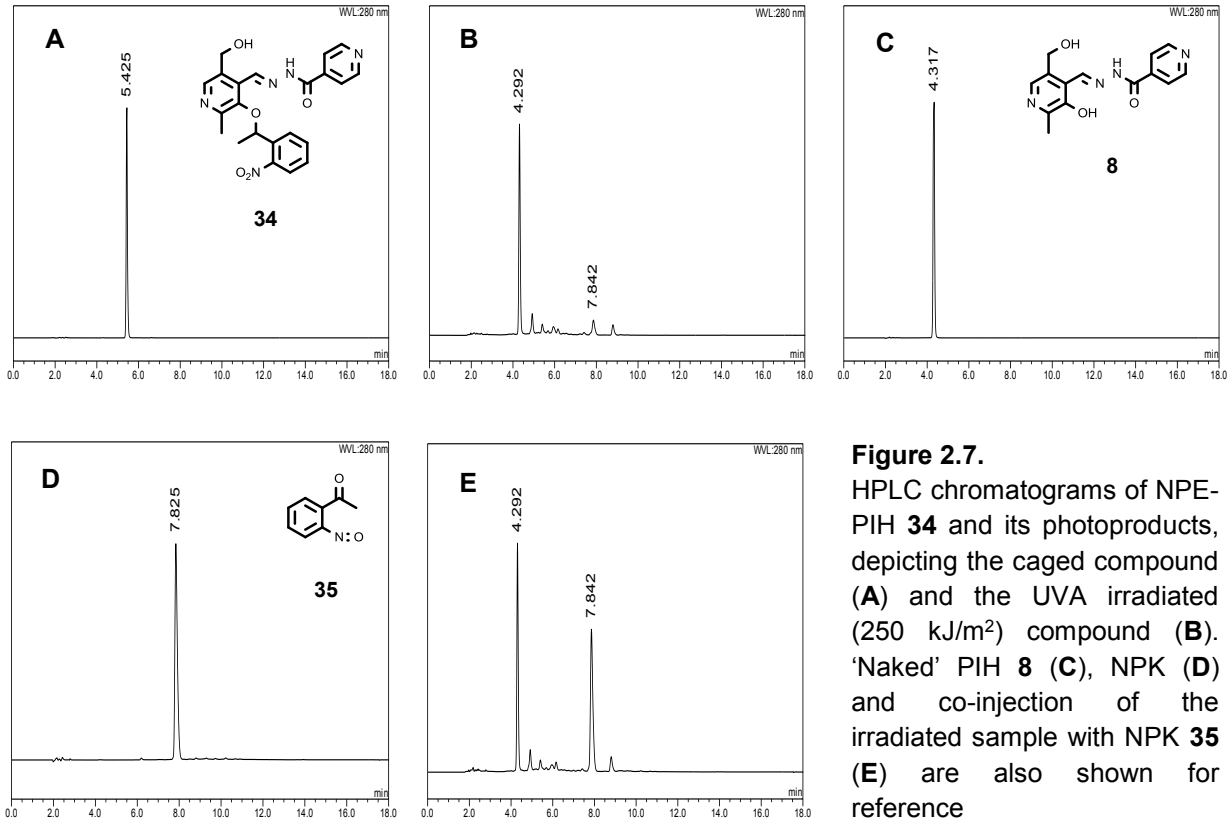


**Figure 2.7.**
HPLC chromatograms of NPE-PIH **34** and its photoproducts, depicting the caged compound (**A**) and the UVA irradiated (250 kJ/m$^2$) compound (**B**). 'Naked' PIH **8** (**C**), NPK (**D**) and co-injection of the irradiated sample with NPK **35** (**E**) are also shown for reference

Similarly, NPE-NIH **53** exhibited decaging which is consistent with our expectations, in that total photolysis occurs at a UVA dose of 250 kJ/m$^2$ and that the 'naked' NIH molecule along with NPK are released (Figure 2.8)

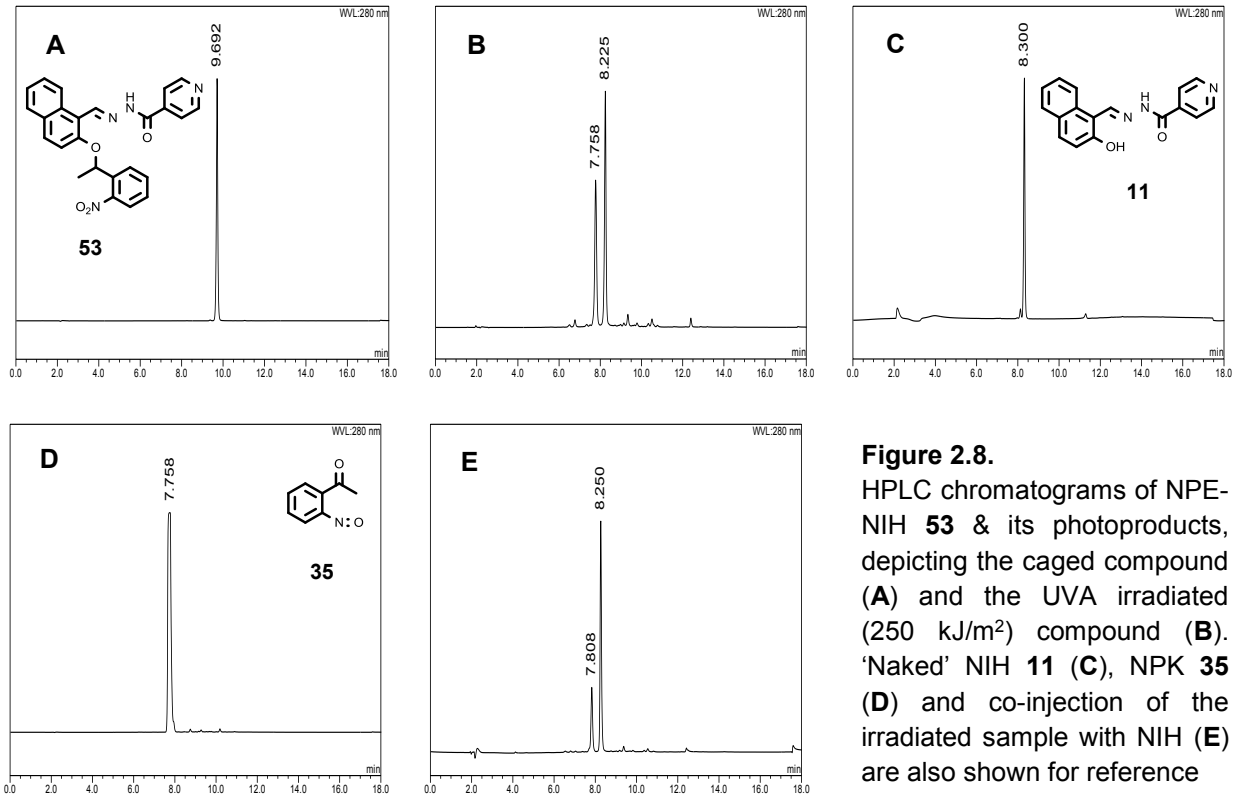


**Figure 2.8.**
HPLC chromatograms of NPE-NIH **53** & its photoproducts, depicting the caged compound (**A**) and the UVA irradiated (250 kJ/m$^2$) compound (**B**). 'Naked' NIH **11** (**C**), NPK **35** (**D**) and co-injection of the irradiated sample with NIH (**E**) are also shown for reference

The NPE-caged thiosemicarbazone compound **55a**, (Figure 2.9) appears to undergo relatively clean photolysis to yield the naked IC and NPK (**B**), as evident from reference chromatograms of the free chelator molecule (**C**) and NPK (**D**). As before, the identity of the signal with a retention time ($R_t$) of 9.1 min is confirmed as the free IC by co-injection of **54a** with the irradiated sample (**E**). Interestingly, photolysis does not appear to fully occur at a dose of 250 kJ/m$^2$ however, as a signal which corresponds to the caged compound remains after irradiation (**B**).

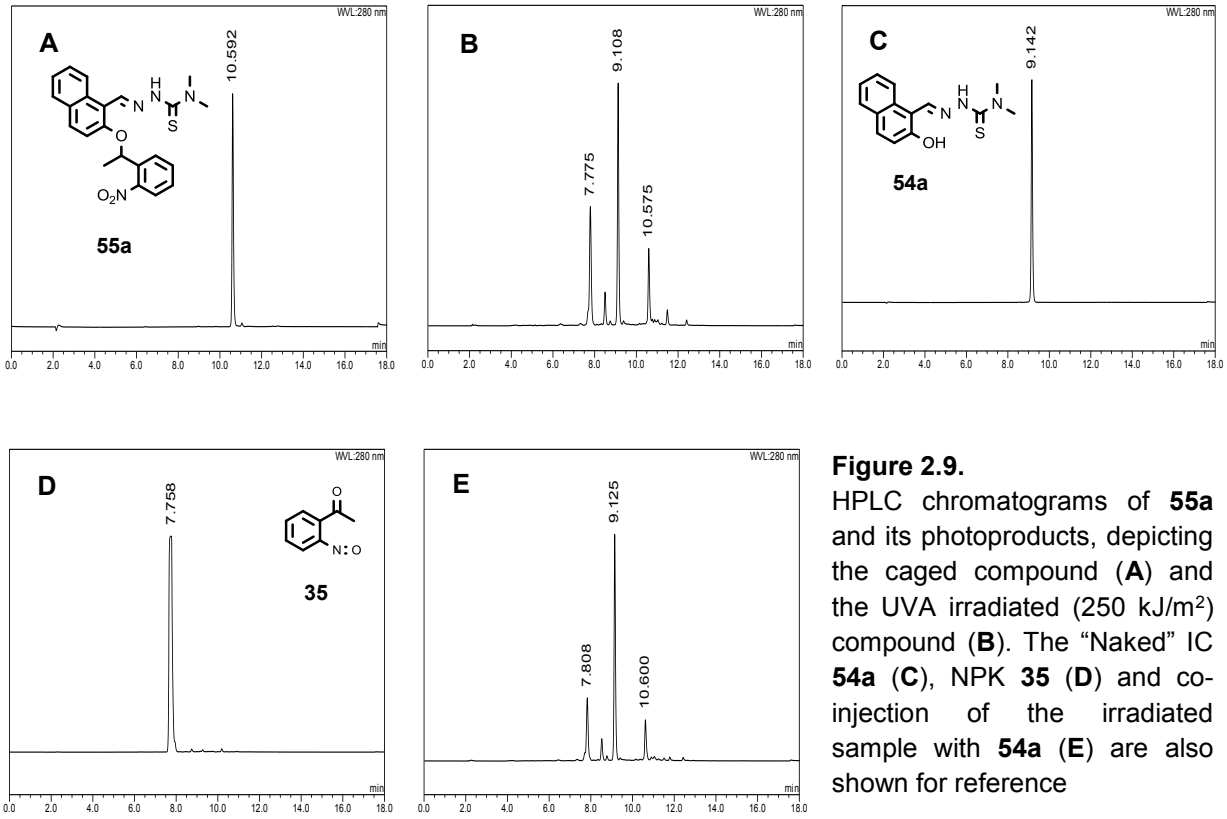


**Figure 2.9.**
HPLC chromatograms of **55a** and its photoproducts, depicting the caged compound (**A**) and the UVA irradiated (250 kJ/m$^2$) compound (**B**). The "Naked" IC **54a** (**C**), NPK **35** (**D**) and co-injection of the irradiated sample with **54a** (**E**) are also shown for reference

Despite only partial photolysis being observed, this compound has two absorption maxima at 238 and 360 nm, with a molar extinction coefficient, $\varepsilon$ of 39786 and 15017 L mol$^{-1}$ cm$^{-1}$ respectively. As this would indicate a reasonable level of absorption within the UVA range, and is comparable with the absorption profiles of the other NPE-CICs described in this chapter, it is surprising that this compound does not undergo complete decaging.

The other NPE-caged thiosemicarbazone compound **55b** (Figure 2.10, **A**) exhibits more favourable photolytic behaviour following irradiation (**B**) as photocleavage occurs fully and cleanly, with only two photoproducts released which are identified as the naked IC (**C**) and NPK (not shown) which can be attributed to the signal at 7.8 min in line with the reference samples already shown.

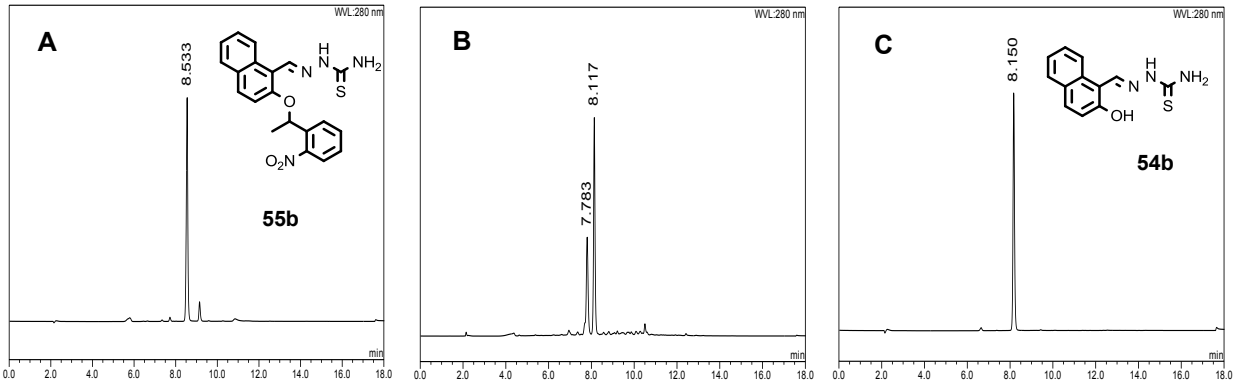


**Figure 2.10.** HPLC chromatograms of the NPE-NT compound **55b** and its related photoproducts, depicting the caged compound (**A**) and the UVA irradiated (250 kJ/m$^2$) compound (**B**). The "naked" IC molecule **54b** is shown for reference (**C**).

With the NPE-caged thiohydrazone analogue of PIH, $H_2$PTBH (**57**), it appears that the extent of photolysis is relatively high (Figure 2.11), owing to a considerable reduction in the signal intensity of the intact caged compound (**A** $\rightarrow$ **B**). It is likely that the new signal with an $R_t$ value of 7.78 min is NPK (**B**); however the identity of the new signal with an $R_t$ value of 6.43 min is uncertain as this differs from the reference value of the 'naked' chelator molecule by 0.25 min (**C**), a significant difference. On the other hand, co-injection of the irradiated sample with the "naked" IC (**56**) shows the appearance of no additional signals, suggesting that the signal with an $R_t$ value of 6.4-6.5 min is derived from the free chelator. Significantly, the appearance of a signal with an $R_t$ value of 5.66 min (**B**) cannot be attributed to any of the expected photoproducts, suggesting that additional photoproduct generation occurs following irradiation of this compound.

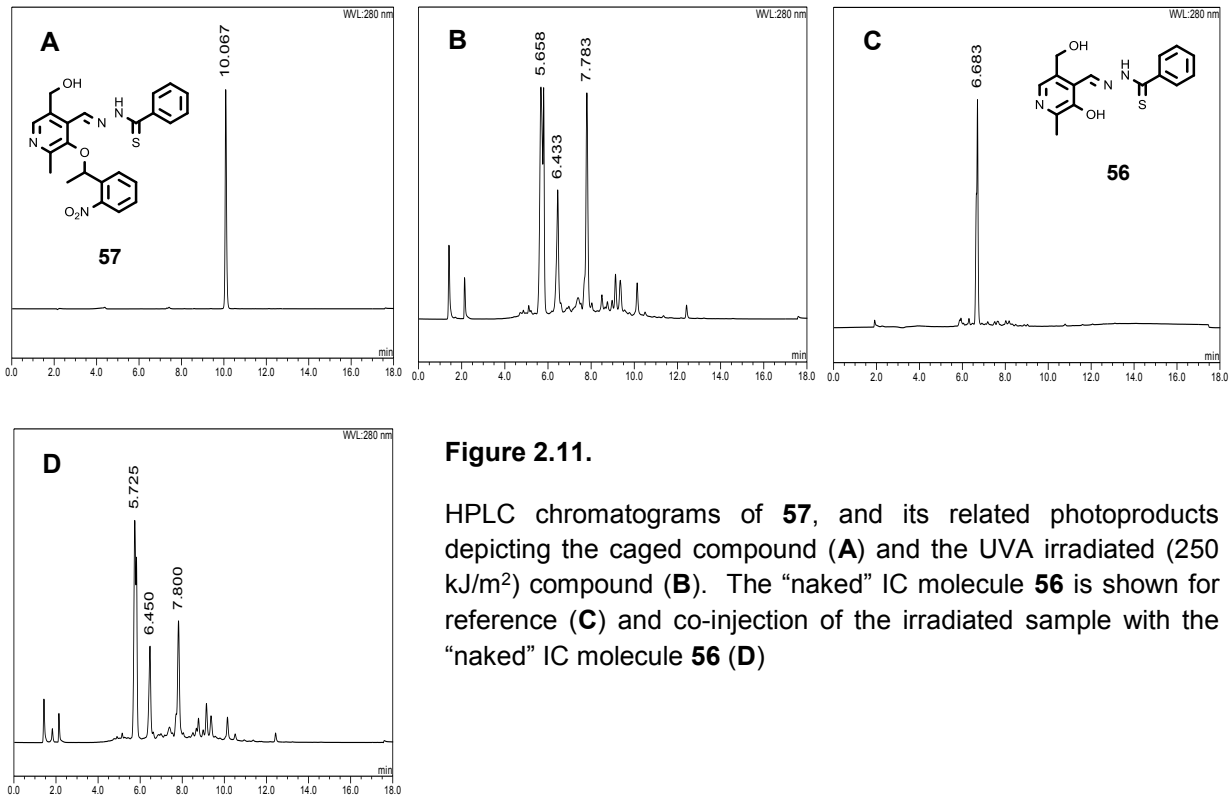


**Figure 2.11.**

HPLC chromatograms of **57**, and its related photoproducts depicting the caged compound (**A**) and the UVA irradiated (250 kJ/m$^2$) compound (**B**). The "naked" IC molecule **56** is shown for reference (**C**) and co-injection of the irradiated sample with the "naked" IC molecule **56** (**D**)

*2.5.6. NV-caged aroylhydrazones*

The decaging profiles of nitroveratryl (NV) caged aroylhydrazones are shown below, namely NV-SIH (**66**, Figure 2.12) and NV-PIH (**67**, Figure 2.13). NV-SIH **66** is shown in the dark and after irradiation (**B**), and it can be seen that photolysis occurs completely and in a relatively clean fashion, with the new major signal appearing to correspond with SIH as expected (**C**). The other minor signal (**B**) is likely to represent the formation of the nitrosobenzaldehyde photoproduct.

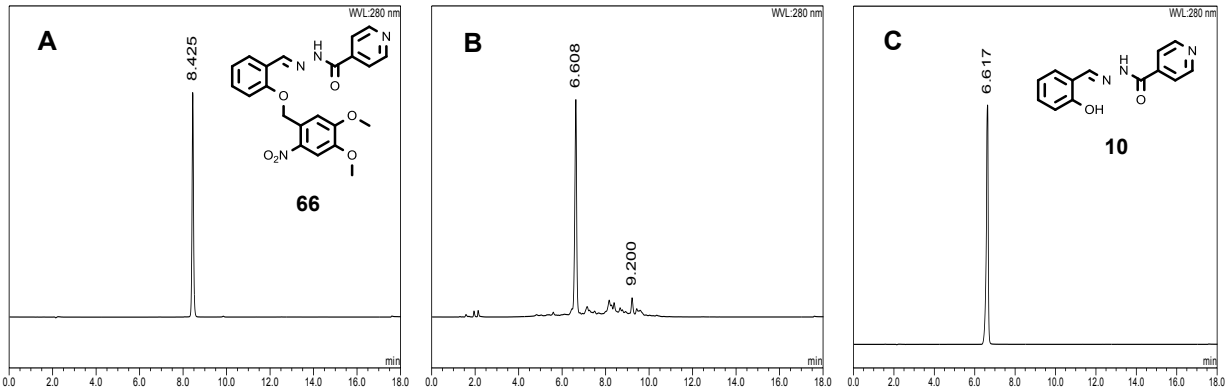


**Figure 2.12.** HPLC chromatograms of NV-caged SIH **66** and its photoproducts, depicting the caged compound (**A**) and the UVA irradiated (250 kJ/m$^2$) compound (**B**). The 'naked' SIH molecule **10** is shown for reference (**C**).

Similarly, NV-PIH **67** (Figure 2.13) decages to liberate PIH (**A** $\rightarrow$ **B**) which is evident from the reference chromatogram of PIH (**C**); however as with irradiation of NV-SIH the formation of nitrosobenzaldehyde is not obvious from these chromatograms, suggesting that this compound merely has low absorbance at 280 nm.

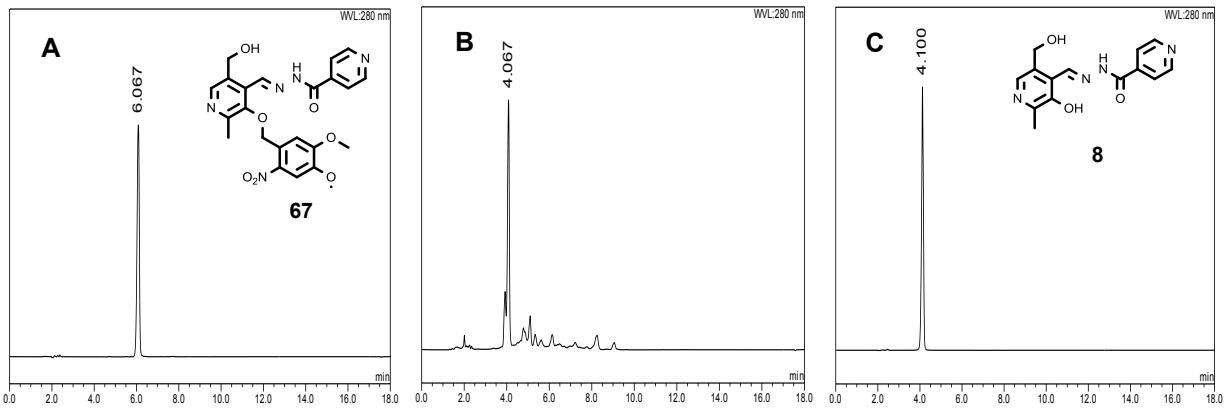


**Figure 2.13.** HPLC chromatograms of NV-caged PIH **67** and its related photoproducts, depicting the caged compound (**A**) and the UVA irradiated (250 kJ/m$^2$) compound (**B**). The 'naked' PIH molecule **8** is shown for reference (**C**).

*2.5.7. DEACM-caged aroylhydrazones*

Irradiation of the 7-diethylaminocoumarin-4-ylmethyl (DEACM) caged compounds are shown below. Interestingly, for DEACM-SIH **78** the product appears to undergo only partial photocleavage at 250 kJ/m$^2$ (Figure 2.14) as the signal relating to the caged compound (**A**) remains even after irradiation, although a signal relating to SIH (**C**) appears to be present, suggesting that a relatively low level of photorelease has taken place.

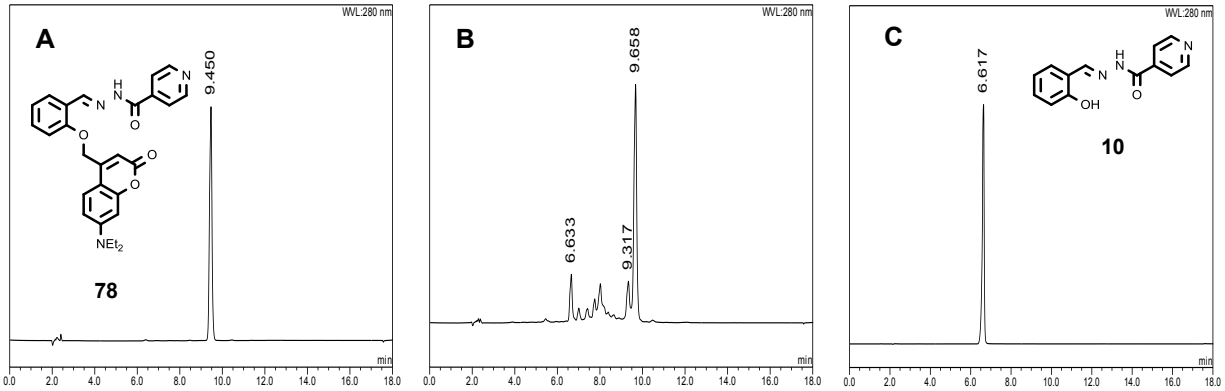


**Figure 2.14.** HPLC chromatograms of DEACM-caged SIH **78** and its related photoproducts, depicting the caged compound (**A**) and the UVA irradiated (250 kJ/m$^2$) compound (**B**). The 'naked' SIH molecule **10** is shown for reference (**C**).

DEACM-caged PIH **75**, the decaging profile of which is shown in Figure 2.15 exhibits similar behaviour to its SIH counterpart, as it is evident that a significant amount of intact caged compound (**A**) remains after irradiation (**B**), although a degree of PIH release has taken place (**C**).

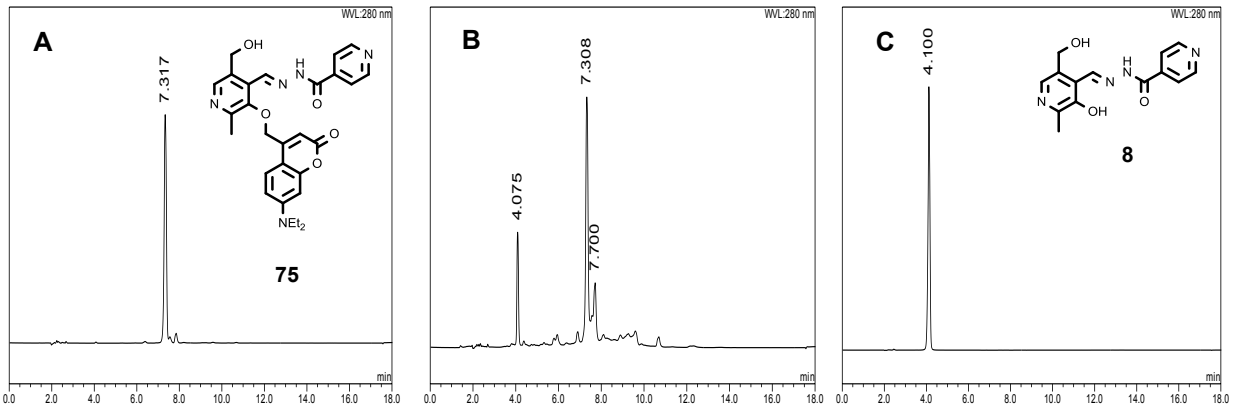


**Figure 2.15.** HPLC chromatograms of DEACM-caged PIH **75** and its related photoproducts, depicting the caged compound (**A**) and the UVA irradiated (250 kJ/m$^2$) compound (**B**). The 'naked' PIH molecule **8** is shown for reference (**C**).

As the UV absorption profile of DEACM-CICs **75** and **78** are considerably red-shifted compared to the NPE and NV-CICs, irradiation with a light source of longer wavelength may result in more extensive photolysis. In fact, the wavelength-selective photolysis of a mixture of NPE and DEACM compounds has been described by Imperiali *et al*. by sequentially irradiating at 360 and 420 nm.[141]

## 2.6. Biological experiments: background

For experimental and methodology details, see experimental section 6.4.

### *2.6.1. MTT assay*

Relative cytotoxicity was measured by MTT assay, which uses the tetrazolium dye 3-(4,5-dimethyl-2-thiazolyl)-2,5-diphenyl-2H-tetrazolium bromide (MTT, **81**) which is reduced by cellular dehydrogenases to the purple formazan **82** (Scheme 2.21).[143]

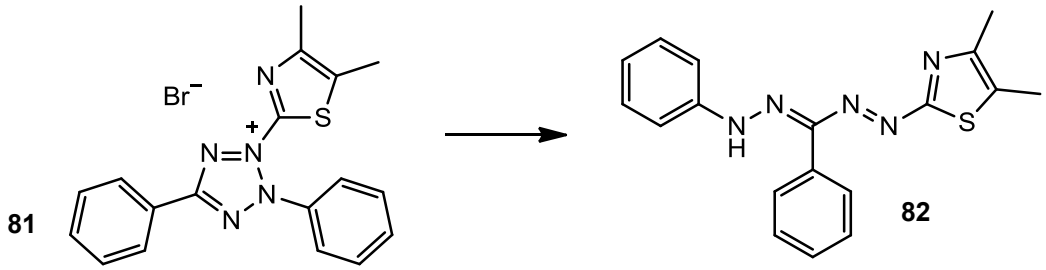


**Scheme 2.21.** Enzymatic reduction of the tetrazole MTT **81** to its purple formazan product **82**

The amount of formazan produced can be measured colorimetrically, which gives a measure of metabolic activity within the cell and is therefore directly proportional to the viable cell number. Thus, when MTT assays are performed with cells that are incubated with compounds of interest, it can be used to deduce the relative cytotoxicity of these compounds.

### *2.6.2. BrdU assay*

The BrdU assay uses the synthetic nucleotide analogue 5-bromo-2'-deoxyuridine, (**83,** Figure 2.16) which gives the assay its name. During the S phase of the cell cycle, this analogue is incorporated into the newly replicated DNA of dividing cells instead of thymidine. BrdU-specific antibodies bind to this nucleotide analogue, and a second antibody conjugated to

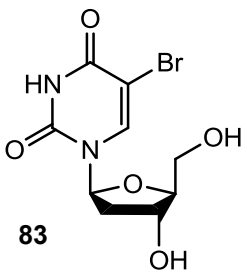


**Figure 2.16.** Structure of BrdU

fluorescein isothiocyanate (FITC) then successively binds to the BrdU-specific antibody. Thus, cells which were actively replicating their DNA can be detected by fluorescence of the FITC marker.

### *2.6.3. Clonogenic (colony forming) assay*

The clonogenic assay (colony forming assay, CFA) is the most reliable way to evaluate viable cell number, and is based on a single cell's ability to grow into a colony, where a colony consists of 50 or more cells.[144]

2.7. Biological experiments: results and discussion.

*2.7.1. Toxicity of parental iron chelators in HaCaT cells*

The relative toxicity of PIH and SIH in the HaCaT cell line are already known from previous studies conducted in the Pourzand laboratory, with $IC_{50}$ values of 100 μM and 20 μM respectively (data not shown).[145] The biological activity of the remaining ICs described within this chapter have not been evaluated however in this cell line

The effect of the aroylhydrazone NIH **11**, the thiosemicarbazones **54a-b**, and the PIH-thiohydrazone analogue $H_2$PTBH **56** on HaCaT cell growth at various concentrations and incubation times is shown below (Figures 2.17-2.20). As one might anticipate, the inherent toxicity or growth-inhibitory effect of these compounds appears to be time dependent, as growth is significantly reduced in cells incubated for 72 h compared to those treated for just 24 h, and this is seen in at least two different corresponding concentrations.

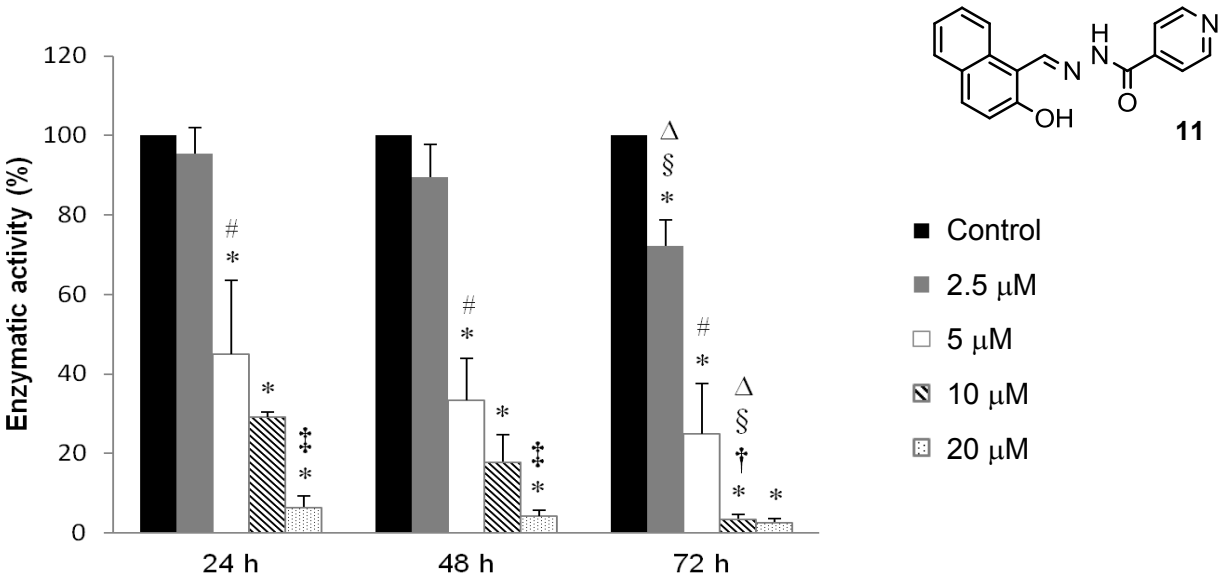


**Figure 2.17.** MTT assay: toxicity of **11** in HaCaT cells after incubation for 24, 48 or 72 h (n = 3-5)
∗ $p < 0.05$, significantly different from corresponding untreated controls.
# $p < 0.05$, significantly different from treatment with **11** at 2.5 μM at same timepoint.
† $p < 0.05$, significantly different from treatment with **11** at 5 μM at same timepoint
‡ $p < 0.05$ significantly different from treatment with **11** at 10 μM at same timepoint
§ $p < 0.05$ significantly different after treatment with **11** for 24 h at same concentration
Δ $p < 0.05$ significantly different after treatment with **11** for 48 h at same concentration

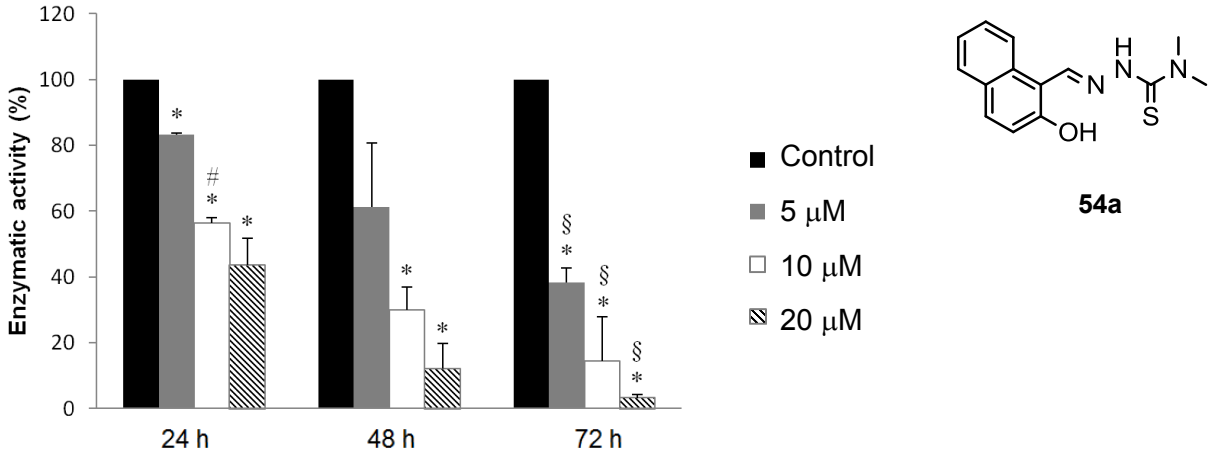


**Figure 2.18.** MTT assay: toxicity of **54a** in HaCaT cells after treatment for 24, 48 or 72 h (n = 3-5)
∗ p < 0.05, significantly different from corresponding untreated controls.
# p < 0.05, significantly different from treatment with **54a** at 2.5 μM at same timepoint.
§ p < 0.05, significantly different after treatment with **54a** for 24 h at same concentration

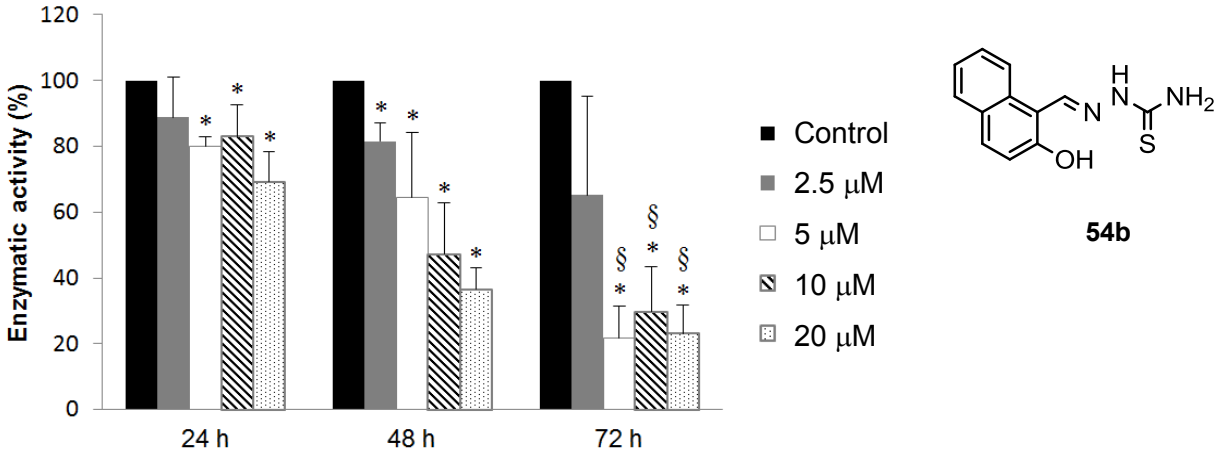


**Figure 2.19.** MTT assay: toxicity of **54b** in HaCaT cells after treatment for 24, 48 or 72 h (n = 3-5)
∗ p < 0.05, significantly different from corresponding untreated controls.
§ p < 0.05 significantly different after treatment with **54b** for 24 h at same concentration

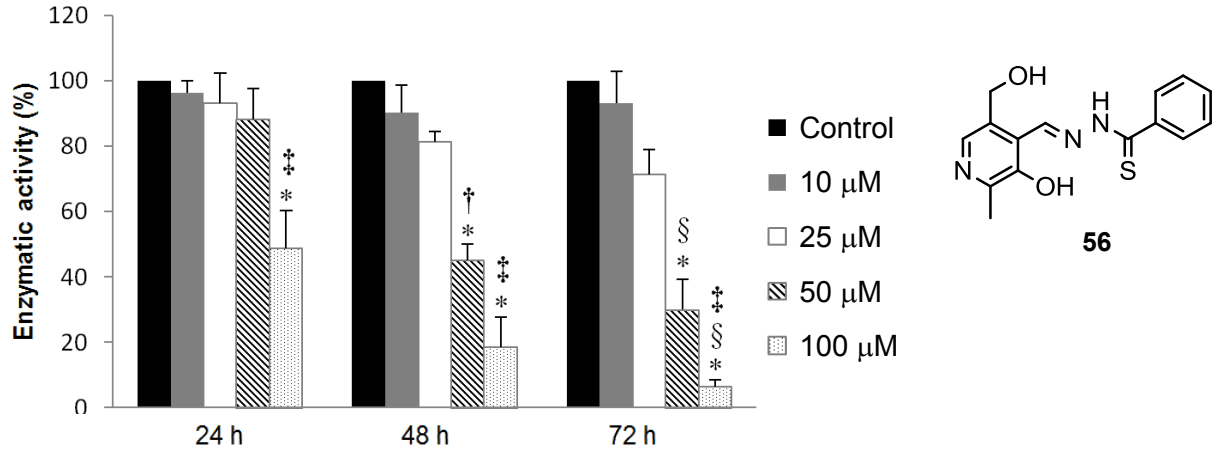


**Figure 2.20.** MTT assay: toxicity of **56** in HaCaT cells after treatment for 24, 48 or 72 h (n = 4)
∗ p < 0.05, significantly different from corresponding untreated controls
† p < 0.05, significantly different from treatment with **56** at 25 μM at same timepoint
‡ p < 0.05 significantly different from treatment with **56** at 50 μM at same timepoint
§ p < 0.05 significantly different from treatment with **56** for 24 h at same concentration

This data are summarised in Figure 2.21. It can be deduced that, after a 72 h incubation time compounds **11**, **54a**, and **54b** have an $IC_{50}$ value of < 5 μM; whereas the $IC_{50}$ values for **8** and **56** are considerably higher, with an $IC_{50}$ of 100 μM for PIH and > 25 μM for $H_2$PTBH (Figure 2.20). These findings are consistent with our expectations, as the more lipophilic compounds such as NIH and NT44mT possess the most cytotoxic effect, whereas the more hydrophilic compound $H_2$PTBH has considerably less potent antiproliferative activity.

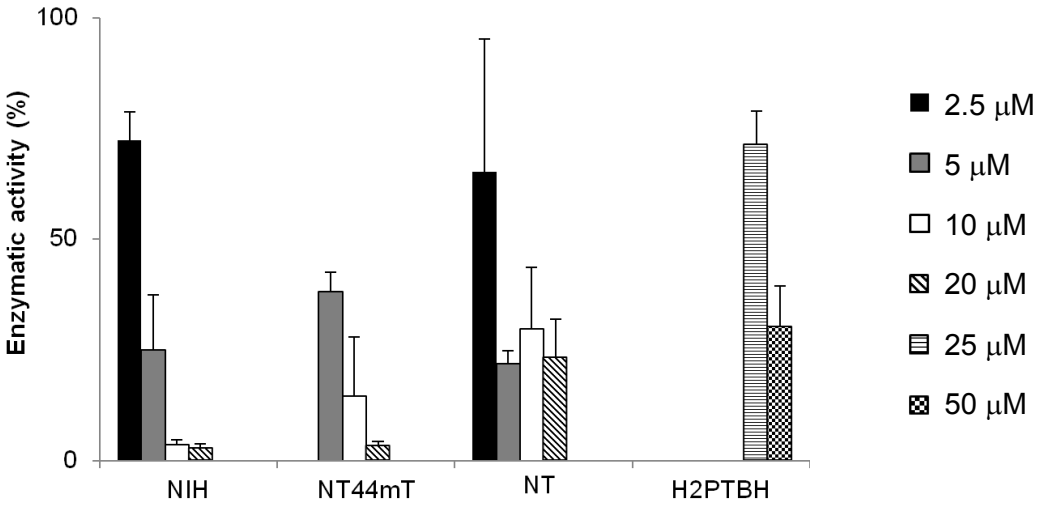


**Figure 2.21.** Summary of growth inhibitory effects of the parental ICs measured by MTT assay: NIH (**11**), NT44mT (**54a**), NT (**54b**) and $H_2$PTBH (**56**).

These results were closely reproduced by the colony forming assay (Figure 2.22). For example, cells treated with the naphthylaldehyde-derived ICs, namely NIH (**11**) NT44mT (**54a**) and NT (**54b**) show a greater reduction in growth rate and colony formation compared to SIH, because of their greater lipophilicity. In agreement with the MTT data, NIH appears elicits the highest degree of cytotoxicity compared to its thiosemicarbazone counterparts NT44mT and NT.

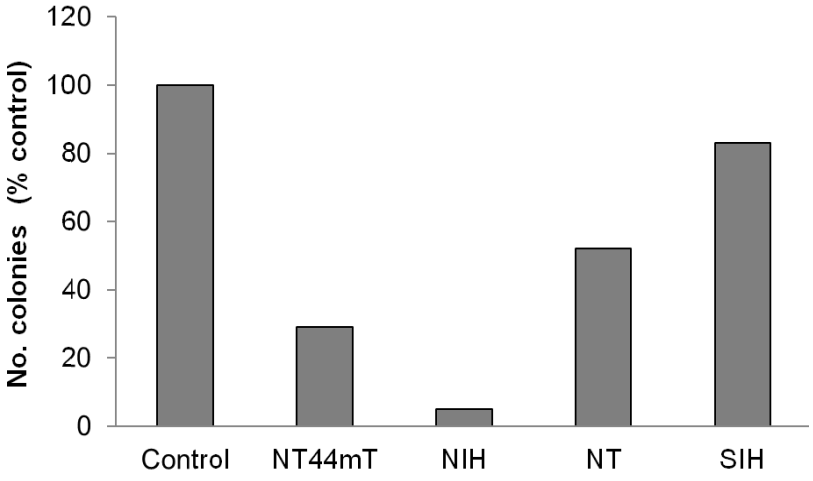


**Figure 2.22.**
Adjusted results of the colony forming assay undertaken with parental ICs (n = 1) at 10 μM.

*2.7.2. Comparative toxicity of CICs and UVA-irradiated CICs by MTT assay*

The growth inhibitory effect of NPE, NV or DEACM-caged CICs in HaCaT cells was evaluated by MTT assay in the same way as described above with the parental ICs. HaCaT cells were treated with the CIC, the corresponding 'naked' IC and the UVA-irradiated CIC which had been irradiated at a dose of 250 kJ/m$^2$. The concentration of compound added was determined by the estimated $IC_{50}$ value deduced from the above experiments. As before, cellular enzymatic activity was measured at 24 h, 48 h or 72 h post-treatment with compounds.

A comparative study with the aroylhydrazones SIH and PIH and their corresponding NPE-caged derivatives **34** and **37** was conducted prior to this project. The results are shown in Figure 2.23, where HaCaT cells were treated with SIH or PIH and their corresponding NPE-caged compounds, along with the respective UVA-irradiated NPE-CICs. All compounds were added at a final concentration of 100 μM; however for these compounds cellular proliferation was only measured 72 h post-treatment.

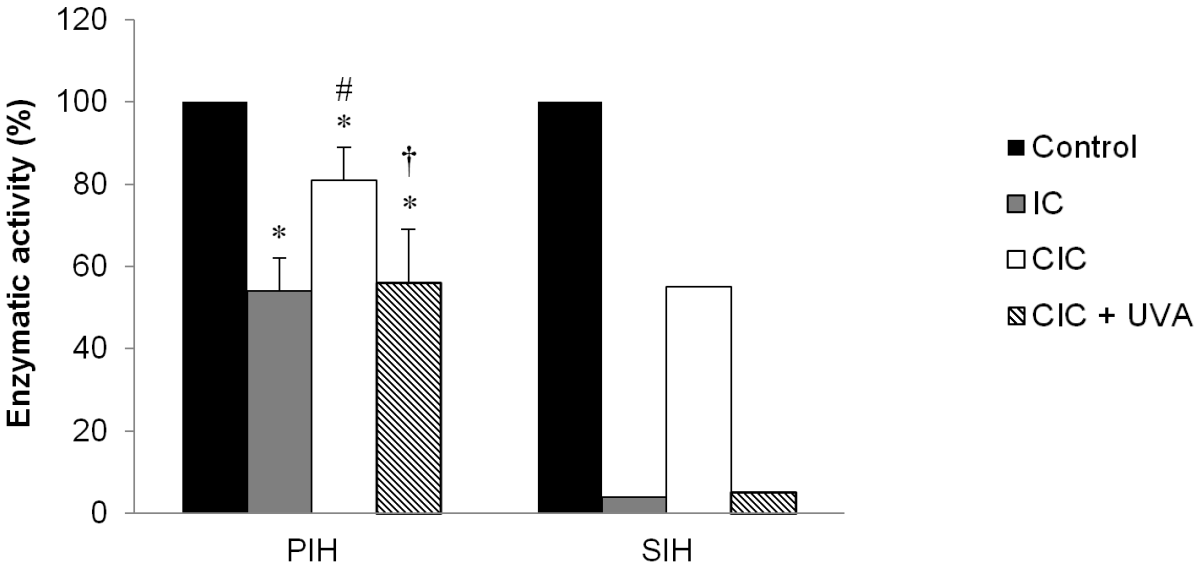


**Figure 2.23.** MTT assay for the 'naked' (IC), NPE-caged (CIC) and UVA-irradiated NPE-caged (CIC + UVA) derivatives of PIH (**8** or **34**) (n = 3-4) and SIH (**10** or **37**) (n = 2) at 100 μM in HaCaT cells 72 h post treatment
*p < 0.05, significantly different from corresponding untreated controls.
# p < 0.05, significantly different from naked chelator at same concentration and same timepoint.
† p < 0.05, significantly different from caged chelator at same concentration and same timepoint

It is apparent that PIH and its derivatives show less toxicity than SIH and its NPE-caged analogue at this concentration, whether irradiated or not. At this

concentration, SIH is considerably more toxic than PIH in this cell line, which is consistent with the notion that increased lipophilicity is associated with more potent cytotoxicity. With both SIH and PIH, the NPE-caged derivative is considerably less toxic than the uncaged parent chelator as anticipated, and upon irradiation this antiproliferative effect appears to be restored to a level which is similar to that of the parental IC

Activity of the CIC compound **53** (NPE-NIH), including the intact (CIC) and UVA-irradiated compound (CIC+UV), along with its 'naked' NIH counterpart in HaCaT cells is shown below in Figure 2.24.

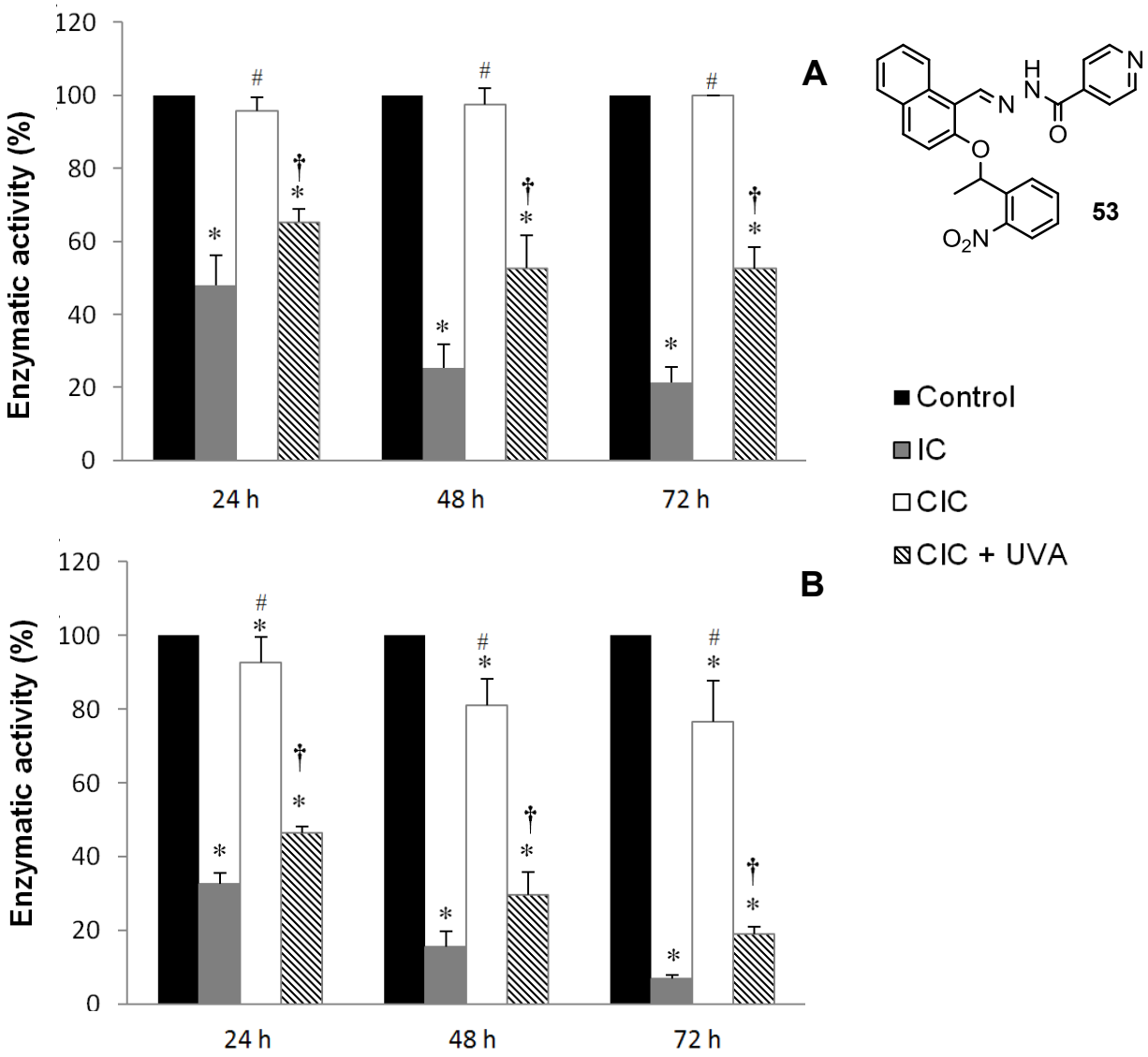


**Figure 2.24.** MTT assay for the parental (IC), NPE-caged (CIC) and UVA-irradiated NPE-caged (CIC + UVA) derivatives of **53** at 5 μM (**A**) and 10 μM (**B**) in HaCaT cells (n = 3).
* $p < 0.05$, significantly different from control cells at same timepoint.
# $p < 0.05$, significantly different from naked chelator at same concentration and same timepoint.
† $p < 0.05$, significantly different from caged chelator at same concentration and same timepoint

As anticipated, the caged compound **53**, possesses the lowest level of toxicity, and after 72 h at 10 μM over 75% of cells remain viable. The 'naked' NIH molecule however possesses marked toxicity compared to its caged counterpart, with significantly higher cytotoxicity apparently observed with longer incubation times and at higher concentrations as one would expect. When **53** is irradiated with UVA at a dose of 250 kJ/m$^2$, an increase in cytotoxicity is observed relative to the 'dark' caged compound and control cells; however the reduction in cell viability never reaches the same level as the naked NIH chelator, which in theory it should providing that complete photolysis takes place. Thus, these results strongly suggest that NPE-NIH remains inactive unless activated by UVA irradiation, where a significant decrease in cellular growth rate occurs which is comparable to that of the free chelator.

Activity of the CIC compound **55a** (NPE-NT44mT), including the intact (CIC) or UVA-irradiated NPE-caged compound (CIC + UV), along with its 'naked' counterpart **54a** is shown below in Figure 2.25. As anticipated, the parental IC exhibits higher toxicity than the NPE-caged compound, however the irradiated compound shows a similar level of toxicity to the intact caged compound. From this, one could deduce that the CIC is simply not decaging; however the decaging profile for this compound (see Figure 2.26) suggests that the 'naked' chelator is indeed released following UVA irradiation as expected. Therefore, assuming that photolysis is proceeding as expected, another explanation is that the NPK fragment may be attenuating the toxicity of the IC following its photorelease.

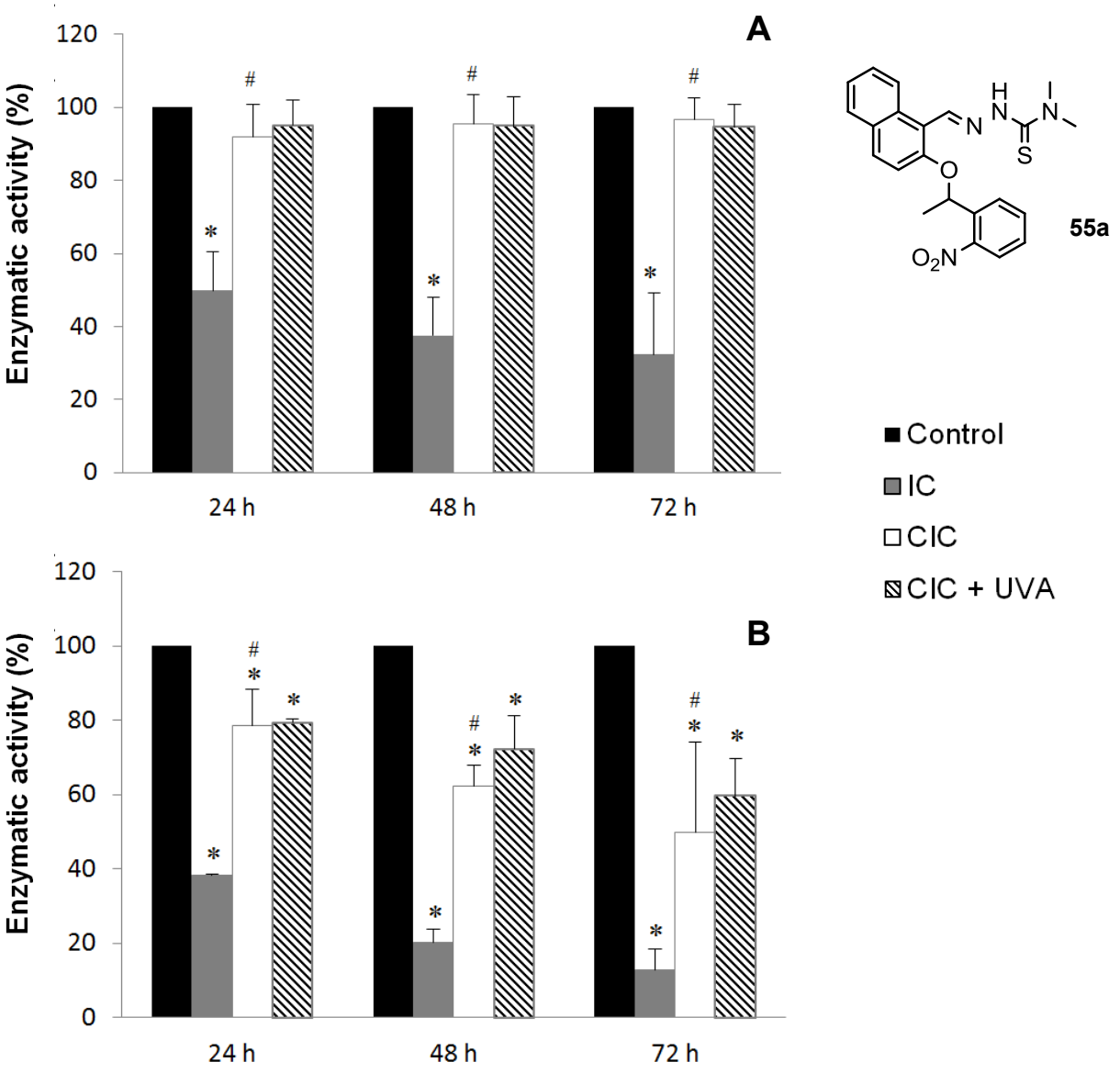


**Figure 2.25.** MTT assay for the parental (IC, **54a**), NPE-caged (CIC, **55a**) and UVA-irradiated NPE-caged (CIC + UVA) derivatives of NT44mT at 10 μM (**A**) and 20 μM (**B**) in HaCaT cells (n = 3)
# $p < 0.05$, significantly different from naked chelator at same concentration and same timepoint.
† $p < 0.05$, significantly different from caged chelator at same concentration and same timepoint

Interestingly, the same pattern is observed with NPE-NT (**55b**) and its derivatives (Figure 2.26), where, again in most cases the UVA-irradiated CIC exhibits a similar level of toxicity to the unirradiated CIC. It is worth noting that this observation is more pronounced in cells treated with the higher concentration (**B**). The decaging profile of NPE-NT shows that photolysis at 250 kJ/m$^2$ is only partial, and so it is reasonable to expect that the level of toxicity observed with the UVA-irradiated compound would not be as marked as that seen with the 'naked' IC molecule, as is apparent at the lower concentration of compound (**A**). This however fails to explain the observations seen when cells are treated with the higher concentration of NT and its derivatives.

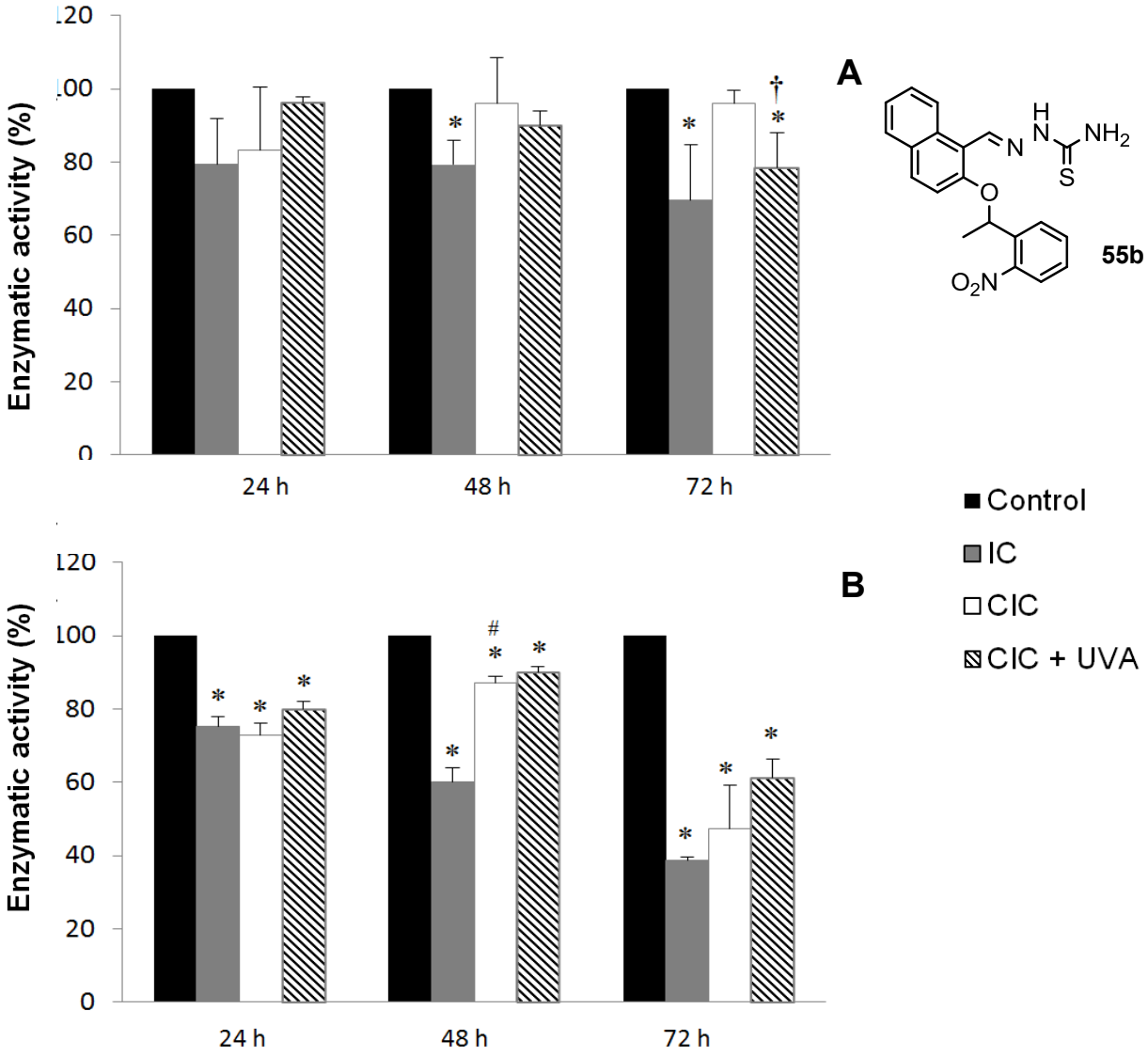


**Figure 2.26.** MTT assay for the parental (IC, **54b**), NPE-caged (CIC, **55b**) and UVA-irradiated NPE-caged (CIC + UVA) derivatives of NT at 5 μM (**A**) and 10 μM (**B**) in HaCaT cells (n = 4)
* $p < 0.05$, significantly different from control cells at same timepoint.
# $p < 0.05$, significantly different from naked chelator at same concentration and same timepoint.
† $p < 0.05$, significantly different from caged chelator at same concentration and same timepoint

Activity of the thiohydrazone-PIH analogue $H_2$PTBH, including the intact (CIC, **57**) or UVA-irradiated NPE-caged compound (CIC + UV), along with its 'naked' counterpart **56** is shown below in Figure 2.27. As anticipated the caged compound **57** exhibits a lower toxicity than its parental counterpart **56**, although this finding is more marked at higher concentrations (**B**). As observed with the thiosemicarbazone derivatives NT44mT and NT, the UVA-irradiated caged compound displays a similar degree of cytotoxicity to the intact or unirradiated caged-compound. The decaging profile for NPE-$H_2$PTBH (**46**) suggests that the expected photoproduct is released, but is accompanied by a considerable level of unexpected photoproduct generation (see Figure 2.11). These additional photoproducts, the identities of which are currently unknown may be responsible for these observations.

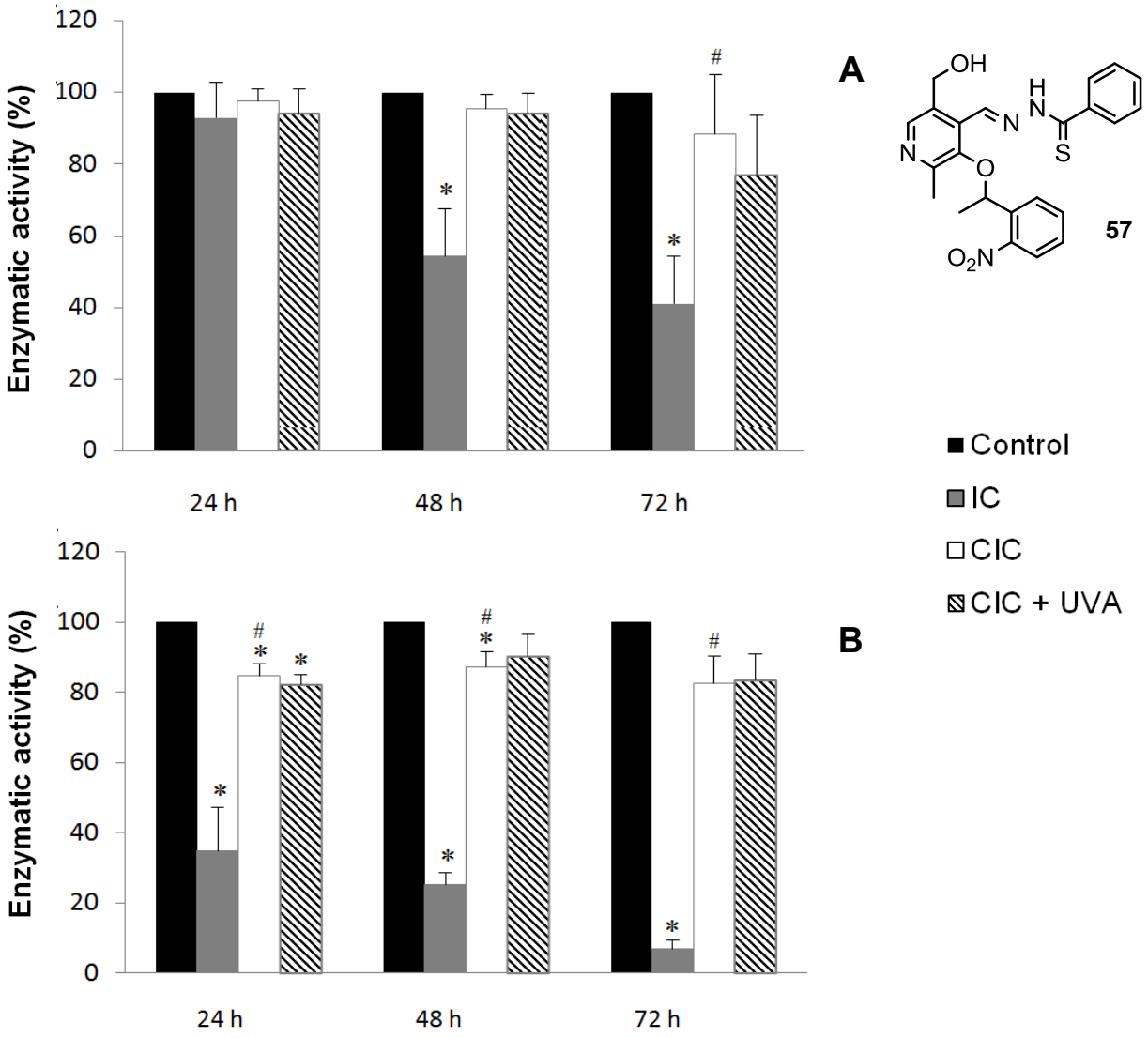


**Figure 2.27.** MTT assay for the 'naked' (IC, **56**), NPE-caged (CIC, **57**) and UVA-irradiated NPE-caged (CIC + UVA) derivatives of $H_2$PTBH at 50 μM (**A**) and 100 μM (**B**) in HaCaT cells (n = 3).
* $p < 0.05$, significantly different from control cells at same timepoint.
# $p < 0.05$, significantly different from naked chelator at same concentration and same timepoint.

Activity of the NV-SIH compound **66**, including the intact (CIC) or UVA-irradiated NPE-caged compound (CIC + UV), along with its 'naked' counterpart is shown below in Figure 2.28. Unexpectedly the NV-caged compound **67** displays higher cytotoxicity than its UVA-irradiated or parental counterpart, which suggest that the caged compound elicits a cytotoxic effect which does not involve cellular iron-binding.

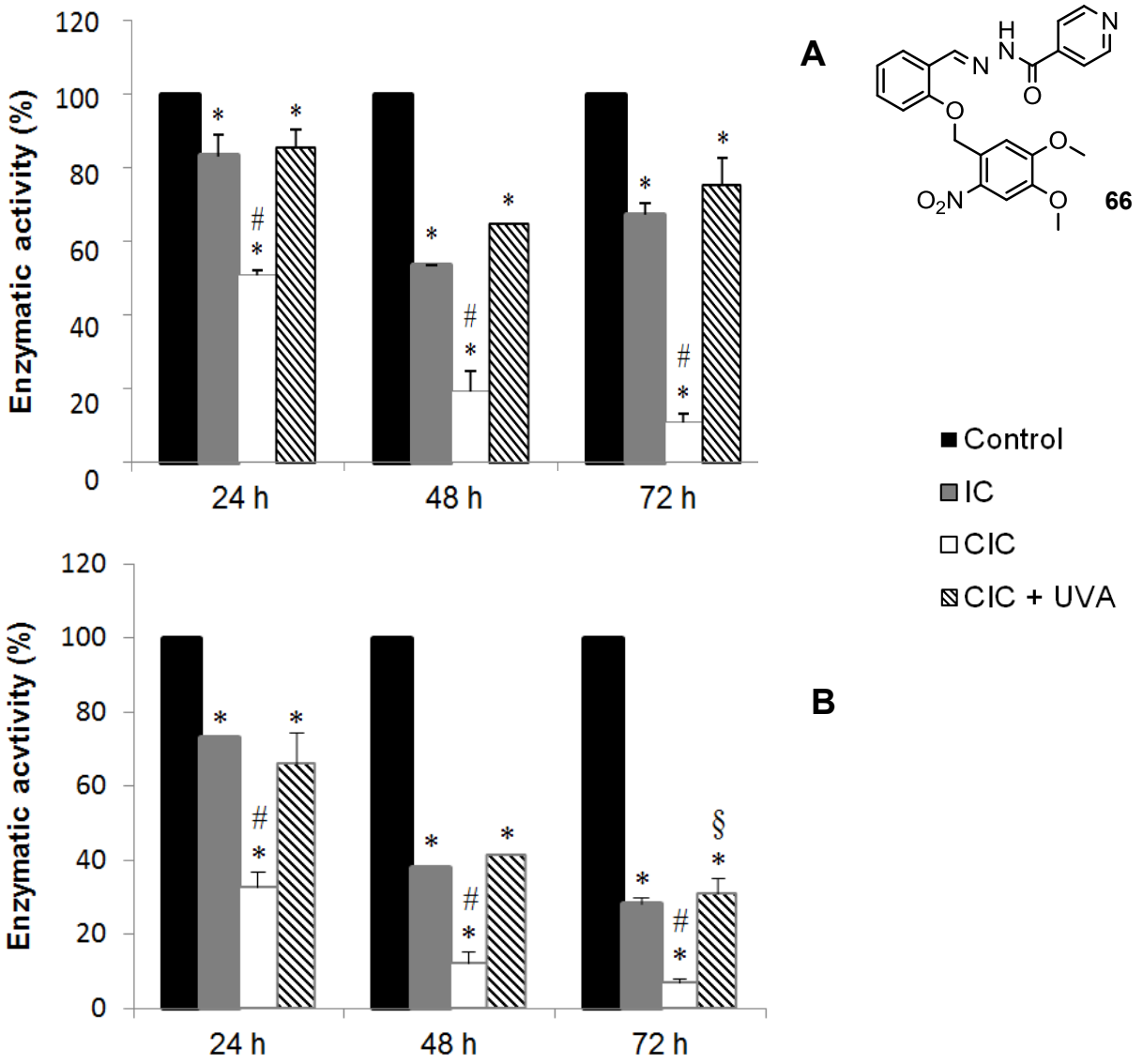


**Figure 2.28.** MTT assay for the 'naked' (IC, **10**), NV-caged (CIC, **66**) and UVA-irradiated NV-caged (CIC + UVA) derivatives of SIH at 20 μM (**A**) and 40 μM (**B**) in HaCaT cells (n = 3).
* $p < 0.05$, significantly different from control cells at same timepoint.
# $p < 0.05$, significantly different from naked chelator at same concentration and same timepoint.
† $p < 0.05$, significantly different from caged chelator at same concentration and same timepoint
§ $p < 0.05$ significantly different after incubation with **66** at 24 h at same concentration

Activity of the NV-PIH compound **67**, including the intact (CIC) or UVA-irradiated NPE-caged compound (CIC + UV), along with its 'naked' counterpart is shown below in Figure 2.29. There were no significant differences between the toxicity of the naked chelator, the NV-CIC, or the UVA-irradiated NV-CIC. Toxicity of the caged compound is neglible, whether UVA irradiated or not, even at the high treatment concentrations used (100 μM).

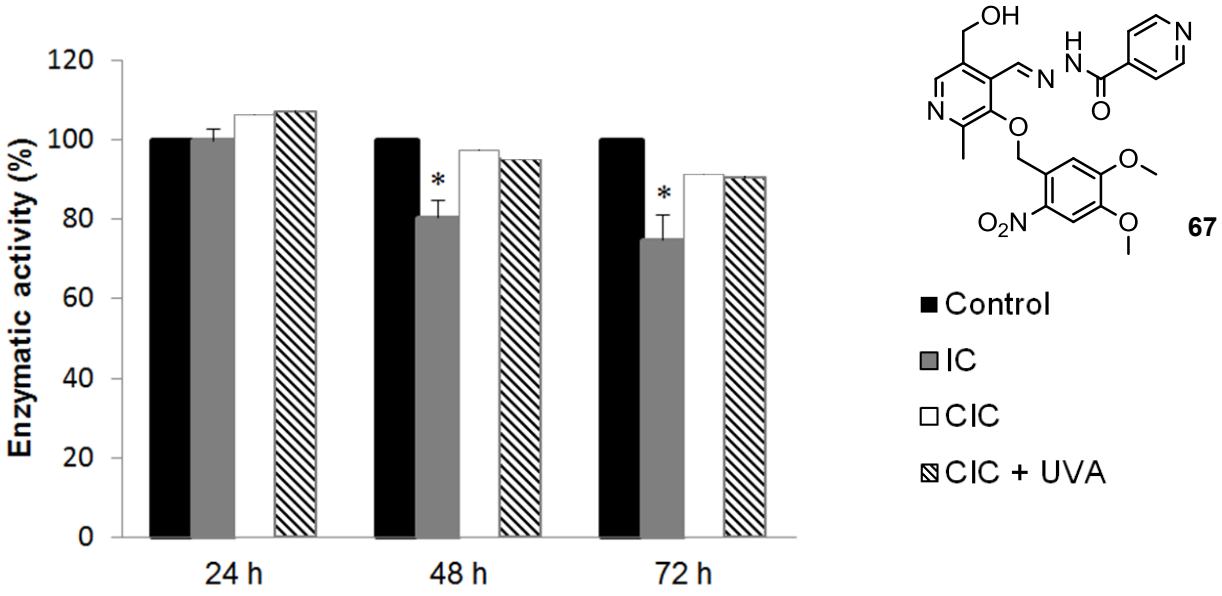


**Figure 2.29.** MTT assay for the 'naked' (IC, **8**), NV-caged (CIC, **67**) and UVA-irradiated NV-caged (CIC + UVA) derivatives of PIH at 100 μM in HaCaT cells (n = 2-3).
* $p < 0.05$, significantly different from control cells at same timepoint.

Activity of the DEACM-caged SIH compound **78** including the intact (CIC) or UVA-irradiated NPE-caged compound (CIC + UV), along with the 'naked' SIH IC **10** is shown in Figure 2.30. As with the other caged-SIH compounds, **78** shows higher toxicity than the parental SIH iron chelator; however, unusually the irradiated CIC exhibits high anti-proliferative activity which does not correspond to the cytotoxicity of SIH. In light of these data however, it should be borne in mind that the decaging profile for this compound (see Figure 2.14) suggested only partial SIH photorelease following UVA-irradiation, along with the generation of additional, unidentified photoproducts. The findings shown below suggest that these additional photoproducts may be toxic, owing to the increase in cellular growth inhibition which is seen in cells treated with the irradiated CIC.

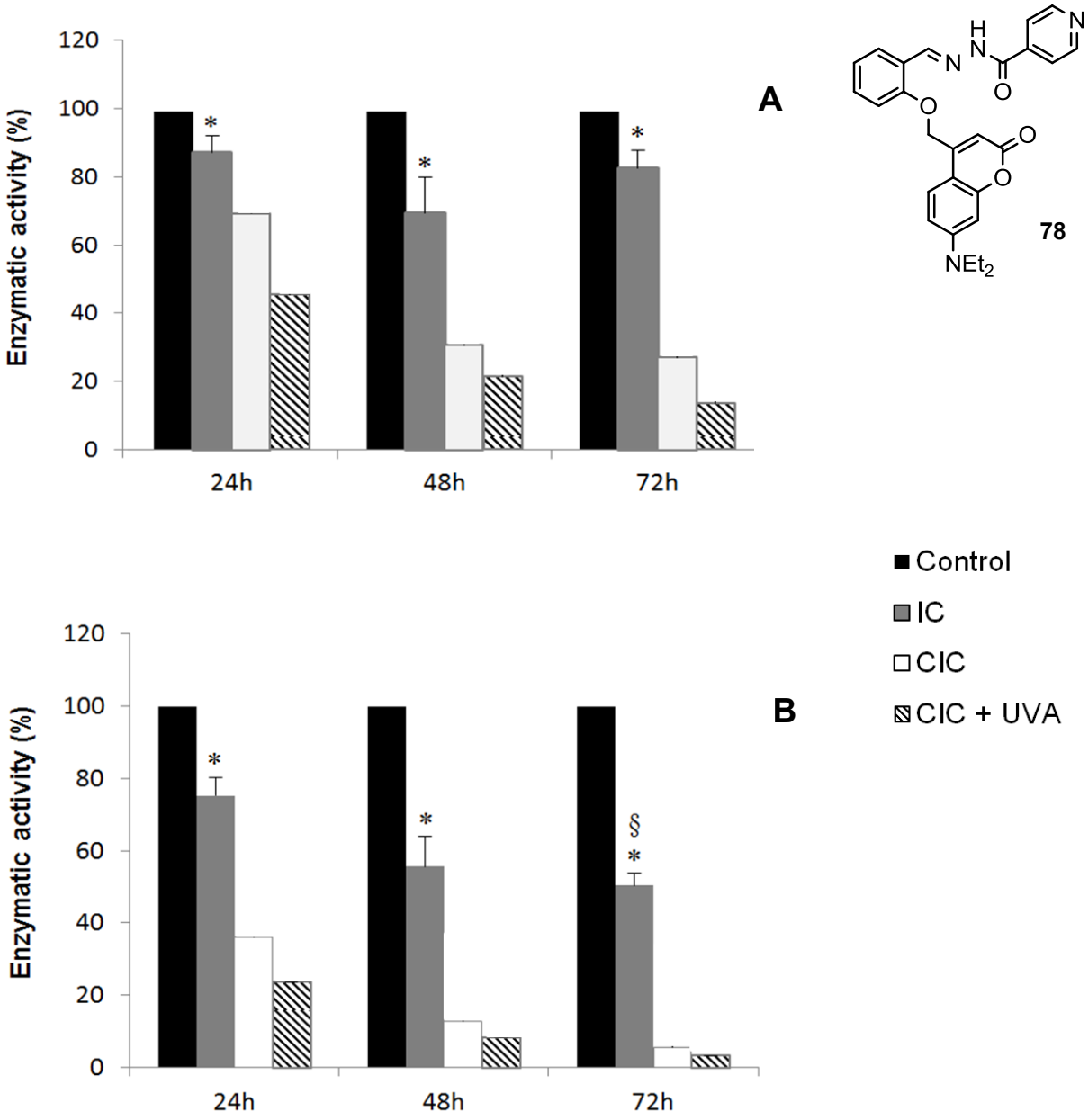


**Figure 2.30.** MTT assay for the 'naked' (IC, **10**), DEACM-caged (CIC, **78**) and UVA-irradiated DEACM-caged (CIC + UVA) derivatives of SIH at 20 μM (**A**) and 40 μM (**B**) in HaCaT cells (n = 2-3).
* $p < 0.05$, significantly different from control cells at same timepoint.
§ $p < 0.05$ significantly different after incubation with **78** at 24 h at same concentration

*2.7.3. Comparative toxicity of CICs and UVA-irradiated CICs by BrdU assay*

The growth inhibitory effect of the aroylhydrazone ICs PIH, SIH and NIH, along with their NPE-caged derivatives and UVA-irradiated NPE-caged derivatives was evaluated by BrdU assay (Figure 2.31, **A**). This was also conducted for the sulfur-containing ICs NT44mT, NT and $H_2$PTBH along with the corresponding NPE-caged derivatives (Figure 2.31, **B**).

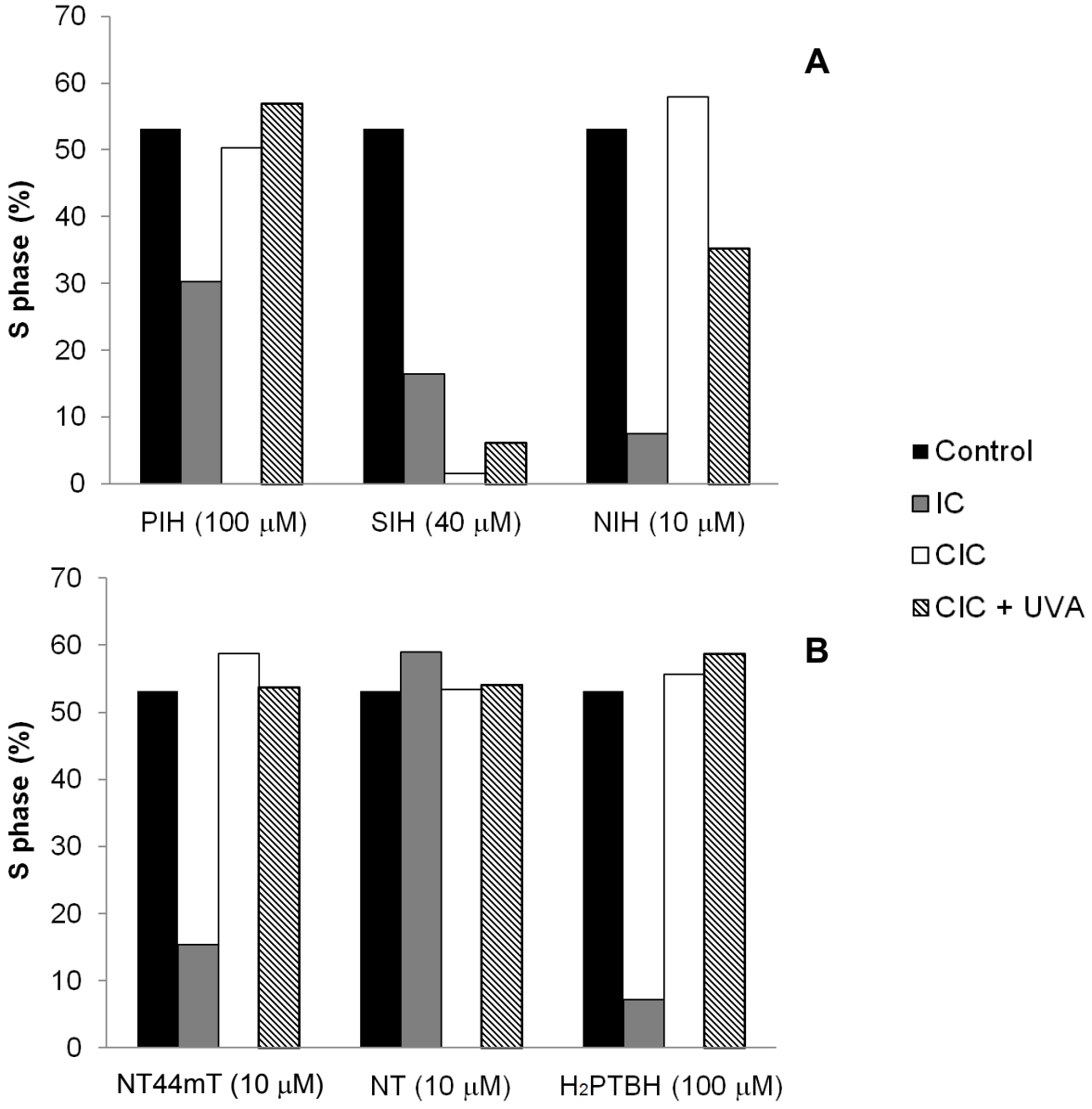


**Figure 2.31.** BrdU assay: Growth inhibitory effect of aroylhydrazones PIH **8**, SIH **10** and NIH **11** (**A**) and sulfur-containing ICs NT44mT and NT (**54a-b** respectively), and $H_2$PTBH **56** (**B**), along with their NPE-caged (CIC) and UVA-irradiated NPE-caged derivatives 72 h post-treatment. (n = 1)

The BrdU assay shows the percentage of cells in S phase, and thus gives a measure of the proportion of cells continuing to undergo DNA synthesis in preparation for mitosis. For the compounds NIH **11**, NT44mT **54a**, NT **54b** and $H_2$PTBH **56**, and their caged derivatives, there is a good degree of correspondence between these results and the growth inhibitory effects measured by MTT assay. The aroylhydrazones PIH and SIH and their derivatives however display activity which differs from that measured with the MTT assay. For example, irradiated NPE-PIH does not appear to exert any biological activity, as a higher percentage of cells treated with irradiated NPE-PIH progress to S phase compared to the untreated controls; furthermore, according to the BrdU data, NPE-SIH displays higher cytotoxicity than the parental SIH chelator.

As shown with the MTT assay, NIH **11** and its NPE-caged derivative **53** shows the most favourable biological profile, as cells treated with the caged compound are more likely to progress to S phase than those treated with the parent or UVA-irradiated caged chelator. Following UVA-irradiation, the cytotoxicity of NPE-NIH does not appear to be fully restored to that of NIH, a finding which was also observed in the MTT assays. This same effect is also displayed with the sulfur-based iron chelators NT44mT **54a** and $H_2$PTBH **56**, where there is no significant difference between cells treated with the caged and UVA-irradiated caged chelators.

*2.7.4. Decaging of NPE-NIH "in vivo"*

The comparative toxicity studies of the caged compounds and their derivatives discussed in the previous section suggest that NPE-NIH exhibits the most attractive biological profile, as its potent cytotoxicity is only observed following UVA irradiation, whereas the intact CIC has no significant antiproliferative effect.

The assays described in section 2.7.3 however use "pre-irradiated" CICs, and cannot be used to show that uncaging of the CIC occurs within cells during exposure to physiologically relevant doses of UVA radiation. This is important as the dose of UVA that a compound is exposed to within a cell will be decreased compared to its irradiation outside a cell, as a significant degree of UVA is absorbed by intracellular chromophores. Therefore, a further experiment was conducted to help demonstrate that NPE-NIH **53** is uncaged within HaCaT cells when the cells are irradiated with UVA. Cells were left untreated (control) or incubated for 72 h following treatment with NIH or NPE-NIH at 5 μM. Cells were then irradiated with UVA at a dose of 50, 100 or 250 kJ/m$^2$, or alternatively not exposed to UVA ('dark'). Figure 2.32 displays the results of the assay.

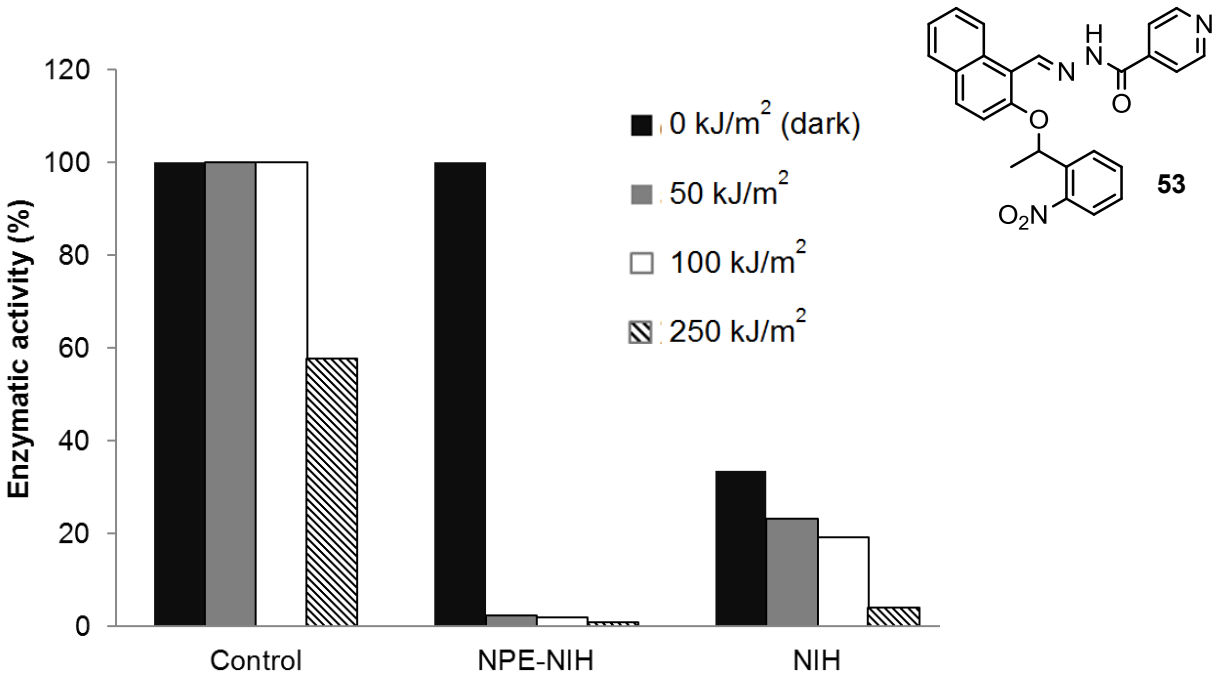


**Figure 2.32.** MTT assay of HaCaT cells in the absence or presence of UVA radiation following treatment with NIH **11** or NPE-NIH **53** at 5 μM. Cells were analysed 72 h post-treatment (n = 1).

HaCaT cells are particularly suitable for this type of experiment, as they demonstrate a high level of resistance to UVA-induced damage, and it is apparent from Figure 2.32 that in control cells which were untreated with compound there are no signs of cell death up to a UVA dose of 100 kJ/m$^2$. Cells which were exposed to the 'naked' NIH iron chelator on the other hand display a marked reduction in cell growth compared to the untreated controls, thus suggesting that the observed cytotoxicity in cells irradiated at low UVA doses is attributable only to NIH. As anticipated, cells treated with the CIC NPE-NIH exhibit no signs of cell death is not exposed to UVA radiation; however at even low doses of UVA radiation (50 and 100 kJ/m$^2$), there is a dramatic reduction in the growth rate of cells, suggesting that uncaging is taking place to liberate the free NIH iron chelator, which is evidently eliciting a potent antiproliferative effect. This data also suggests however that the irradiated cells treated with NPE-NIH are more susceptible to cell death compared to those treated with the naked chelator, and the control cells irradiated at 50-100 kJ/m$^2$ appear to show that such cell damage is not UVA-related.

*2.7.5. Toxicity of nitrosophenylketone (NPK) in HaCaT cells*

NPK (**35**) is one of the two expected photoproducts released following NPE-CIC photolysis with UVA; however there are currently no known studies where the biological effects of NPK in cellular systems are explicitly evaluated. Any activity that NPK exerts on cells however could have a substantial impact on the biological outcome of NPE-CICs, and any results observed from irradiated CICs may not reflect the action of the "active" IC fragment. For this reason, a preliminary assessment of the biological effects of NPK in HaCaT cells was undertaken.

NPK toxicity was evaluated using the MTT assay as previously described. Cells were treated with NPK at 20, 40 or 100 μM and any reductions in growth were measured at 24, 48 and 72 h. In addition, some cells were also treated with SIH, and the thiosemicarbazone chelator NT as a comparison, as well as mixtures of NPK and these ICs which should 'mimic' the release of these fragments following photolysis of the NPE-CIC. The rationale for this was to try and elucidate the comparative toxicity results for the UVA-irradiated sulfur-containing ICs, where in all cases the irradiated CIC did not exhibit the same level of toxicity as the parental chelator. A possibility for this is that the addition of NPK attenuates the activity of the chelator, which could occur through an interaction of the thioamide sulfur and the nitroso function of NPK. The reaction of thiols and nitroso compounds has already been reported by Corrie *et al*., resulting in the formation of a benzisoxazole **85** (Scheme 2.22).[117]

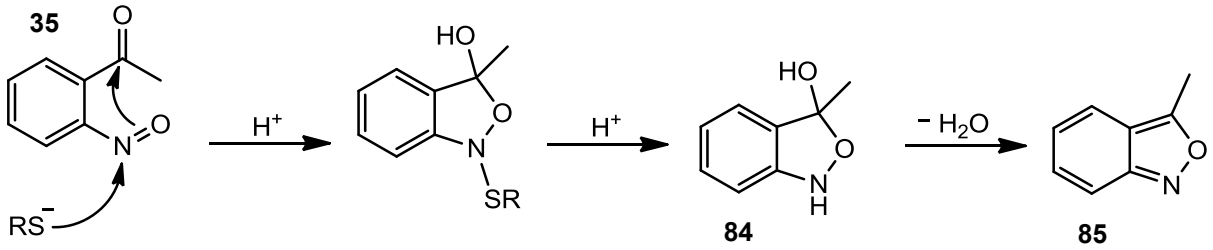


**Scheme 2.22.** Mechanism of NPK reaction with thiolate ion RS to give benzisoxazole **85**, as proposed by Corrie et al. [117]

The results obtained show that NPK elicits relatively low toxicity, as it does not appear to have any significant effect on cell growth at concentrations up to 40 μM (Figure 2.33); however significant toxicity is observed at high concentrations (100 μM). For lipophilic NPE-caged iron chelators, such as SIH and NIH, these results are unlikely to have a significant impact, as the antiproliferative activity of these ICs is apparent at concentrations significantly below those for NPK; however for compounds with less potent antiproliferative effects, such as PIH which has an $IC_{50}$ value of 100 μM in HaCaT cells, any toxic effects observed could be a consequence of NPK and not the IC. Interestingly, this theory is not evident from comparative MTT assay results of PIH and its NPE-caged derivative (Figure 2.24), as the toxicity observed is consistent with that of the parent PIH molecule.

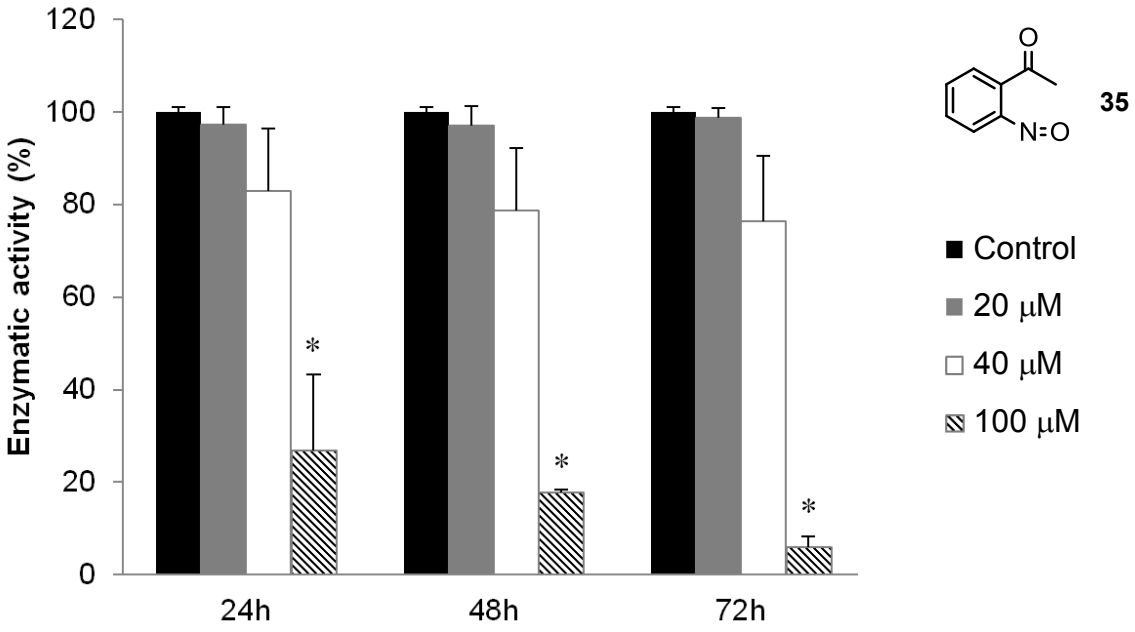


**Figure 2.33.** MTT assay: toxicity of NPK **35** in HaCaT cells after incubation for 24, 48 or 72 h (n = 3). * $p < 0.05$, significantly different from corresponding untreated controls.

Comparison of the growth inhibitory effect of cells treated with NPK and SIH or a mixture of NPK/SIH are shown in Figure 2.34, where at a concentration of 20 μM cells treated with a mixture of NPK and SIH show no significant growth retardation compared to those treated with SIH alone. This is consistent with the results shown in Figure 2.33 that NPK elicits no significant toxicity at 20 μM.

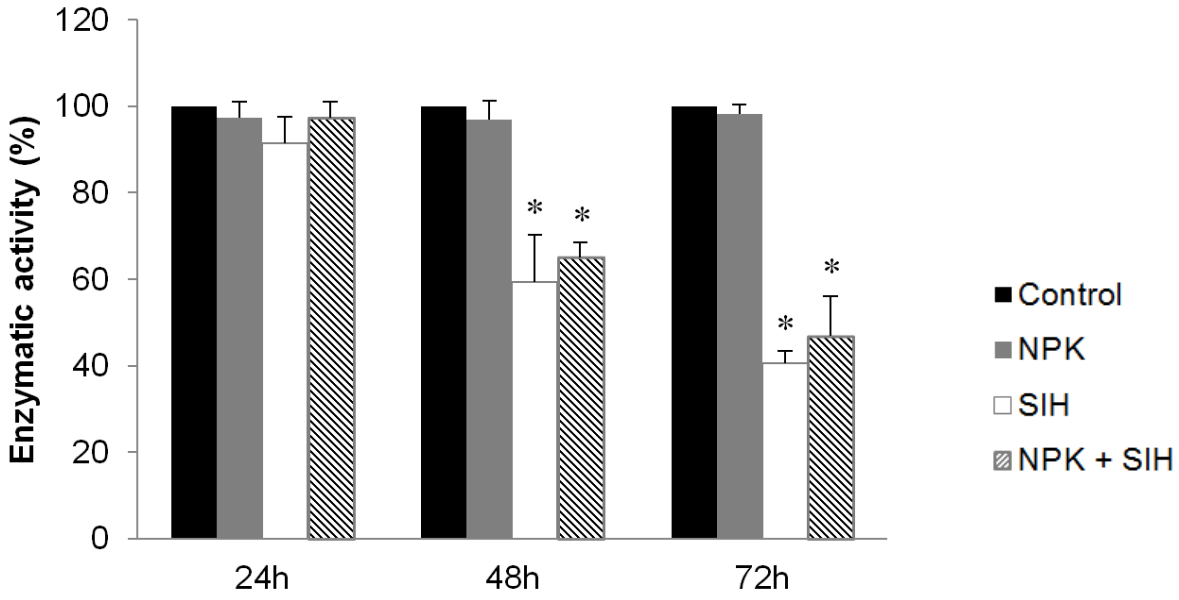


**Figure 2.34.** MTT assay for NPK **35**, SIH **10**, or a mixture of **35/10** at 20 μM in HaCaT cells (n = 3).
∗ $p < 0.05$, significantly different from corresponding untreated controls.

Comparison of the growth inhibitory effect of cells treated with NPK and NT, or a mixture of NPK/NT are shown in Figure 2.35, where it is apparent that a mixture of NPK/NT does not have any significant growth inhibitory effects compared to NT or NPK alone. Furthermore, the degree of toxicity observed in cells after a 72 h treatment time with the NPK/NT mixture appears to correspond to that observed in cells with irradiated NPE-NT at the same timepoint. It fails however to suggest that NPK is attenuating the effects of the sulfur-containing NT chelator, as toxicity is higher in cells treated with a mixture of NPK/NT than NPK alone.

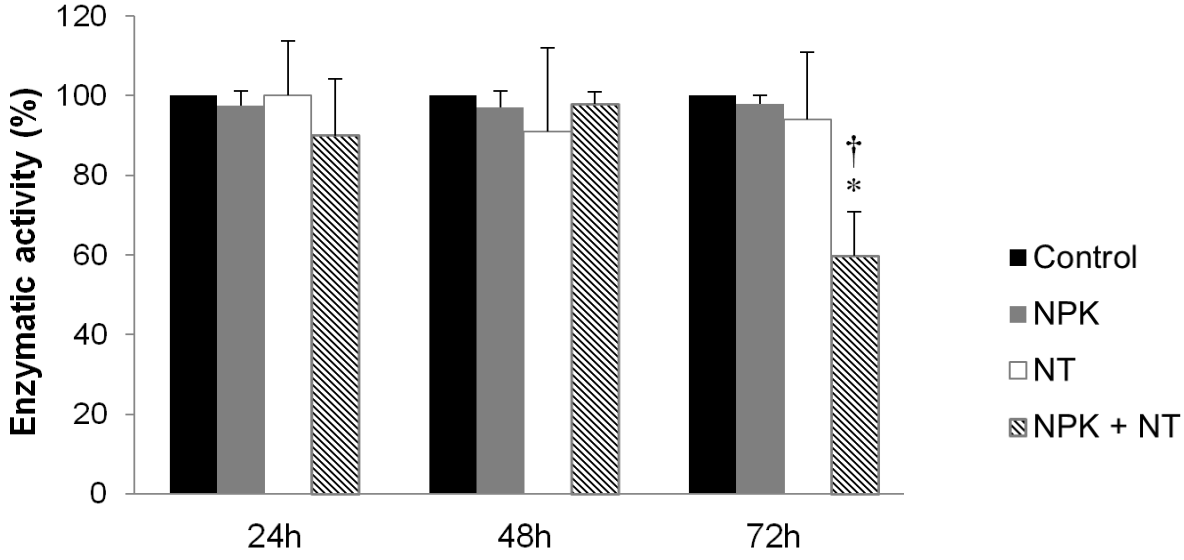


**Figure 2.35.** MTT assay for NPK **35**, NT **54b**, or a mixture of **35/54b** at 10 μM in HaCaT cells (n = 3).
∗ $p < 0.05$, significantly different from corresponding untreated controls.
† $p < 0.05$, significantly different from corresponding NPK-treated cells.

It would therefore appear that there is no interaction between NPK and the NT iron chelator. To confirm this theory, a mixture of NPK and NT were dissolved together in DMSO at a concentration of 0.5 mg/mL, and analysed by HPLC at 4 and 24 h. The chromatogram did not suggest the formation of any new products (not shown).

## 2.8. Future work

The MTT, BrdU and CFA assay results presented in this chapter have helped to elucidate the biological profiles of the CICs described herein, although for many of these compounds the results obtained represent only a preliminary stage of the investigatory work required.

The biological data obtained suggest that the NPE-caged sulfur-based ICs do not exert the expected *in vitro* effects following irradiation with UVA. It has also been observed that aroylhydrazones caged with the NV or DEACM moieties are toxic to the cell lines used, thus suggesting that NPE-CICs possess a more favourable toxicity profile. Further biological assays are required to validate these results, and to identify whether the same effects are observed in an alternative cell line, such as FEK4 fibroblasts for example, or another tumourigenic skin cell line.

Furthermore, decaging profiles of the NPE-CICs appear to show more attractive photolytic behaviour than their NV or DEACM counterparts, and these findings, combined with the synthetic work described has allowed for a proof-of-concept study into the caging of aroylhydrazone ICs and their derivatives with various caging groups. Further studies on the wavelength specific cleavage of DEACM-CICs **75** and **78** are therefore required by utilising a different light source.